2009

R Aquarii: Understanding the mystery of its jets by model comparison

Michelle Marie Risse
Iowa State University

R Aquarii: Understanding the mystery of its jets by model comparison

by

Michelle Marie Risse

A thesis submitted to the graduate faculty

in partial fulfillment of the requirements for the degree of

MASTER OF SCIENCE

Major: Astrophysics

Program of Study Committee:
Lee Anne Willson, Major Professor
Steven D. Kawaler
Craig A. Ogilvie
David B. Wilson

Iowa State University

Ames, Iowa

2009

TABLE OF CONTENTS

LIST OF TABLES

LIST OF FIGURES

CHAPTER 1. Intent

In this research, we examine the unique Mira binary called R Aquarii. The first goal of this research is to get a better understanding of the system. This is done by delving into several scientific papers that pertain to this star. With so many papers to keep track of, a data base is needed to locate, combine, and compare all data available for this system.

To further our understanding, careful study is needed to find out how these two stars interact. Since the star is unresolved, only a few indirect methods can tell us how far apart the stars are and the orientation of their orbit. With what data we do have, we focus our attention on different physical models that pertain to this unique star. Several physical models have been suggested for this binary; however, many dont fit the characteristics of the star. From here, we compare the different models and eliminate candidates from the list.

The final goal is to write this report in a manner that anyone with just a slight background in astronomy could follow along. It is a difficult task to be able to bring the abstract down to a more tangible level. However, this is a crucial task in order to spread knowledge to a more public audience.

CHAPTER 2. Introduction

2.1 What Is R Aquarii?

On a clear night in mid-August, the constellation Aquarius is visible in the south around 10pm. Nestled within this constellation lies the distant star R Aquarii (R Aqr) which the unaided eye would simply glance over. As one can see from Figure 2.1, the star is not one of the brightest stars in the constellation, and it is not a part of the main constellation we know. However, closer examination reveals there is more to this star than meets the eye.

Figure 2.1: The constellation of Aquarius with R Aqr labeled in a highlighted box (Isles, 1994).

The most notable observation is that R Aqr varies in brightness over the course of 387 days, going from an 11th magnitude star to a 6th magnitude star (a change of 100 times in brightness) as seen by the light curve in Figure 2.2. This periodic variability is that of a Mira variable. Mira variables are a class of pulsating variable stars; they are red giants (temperature range of 2000 K – 3500 K) with pulsation periods longer than 100 days and light amplitudes greater than 2.5 in magnitude. They also show emission lines of hydrogen and some other elements during at least part of their pulsation cycle. Named after the star Mira, Mira variables typically are less than two solar masses, and they are several thousand times more luminous than the Sun.

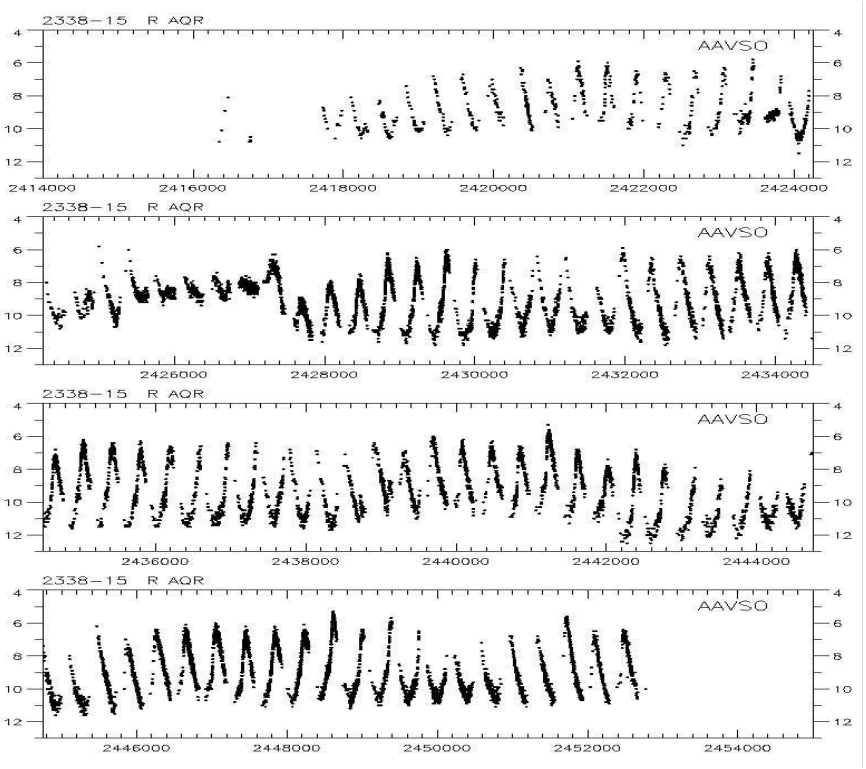

Figure 2.2: Light curve of R Aqr taken from the American Association of Variable Star Observers (AAVSO) International Database.

Viewed from the visual spectrum, R Aqr is classified as a symbiotic system with signatures of both very hot and very cool material; viewed from the infrared, the system may be classified as a dusty-type symbiotic binary. The dusty symbiotic systems are a special subset of Mira

variables. These binaries are a system in which one star has expanded its outer envelope and is shedding mass quickly onto its companion, or are systems in which one star is slowly losing its outer layer and the companion sweeps up the material. The companion is a hot star (often a white dwarf) that is ionizing the gas. Denoted as D-type, the dust surrounding the binary dominates the 1–4 μm spectral range. Like slow novae, the outbursts of these symbiotic novae span many decades. The closest of these stars is R Aqr residing about 250 parsecs away. The preferred interpretation for the R Aqr system is that the Mira has a white dwarf companion, with the unusual time variability associated with the interaction of the two stars (Whitelock, 1987).

2.2 Historical Details

R Aqr was first discovered to be a variable star by Karl Ludwig Harding in 1810. Harding was an assistant at Johann Schroeter's Observatory in Lilienthal, Germany and was a member of the project known as the "Celestial Police." The mission of the Celestial Police was to look for the "missing" planet between Mars and Jupiter. Although the elusive planet was never found, Harding did discover several other objects, including the asteroid Juno in 1809. His observations also led him to discover four variable stars: R Virginis (1809), R Aquarii (1810), R Serpentis (1826), and S Serpentis (1828).

R Aqr was considered to be an ordinary long-period variable for nearly a century. However, in October of 1919 astronomers, using the 100 inch Hooker Telescope and the slit spectrograph on the Mount Wilson Observatory, found several emission lines revealing a hot gaseous nebula in addition to the M7e spectrum of the long-period variable star. M7 is the spectral class of the main star (the red giant star) and the "e" denotes emission lines of hydrogen are present. In 1922, a more complex spectrum was observed and three very different spectra were seen: the M7e star, the nebula, and a blue companion of spectral type O or B, such as a white dwarf (Mattei and Allen, 1979).

The nebulosity surrounding the stars, also known as Cederblad 211, was first seen on photographic plates at the Lowell Observatory in 1912. In 1939, Edwin Hubble detected

the expansion of the nebula using differences between different images taken 17 years apart (Adams, 1942). After Hubble's departure during the war, Walter Baade confirmed Hubble's finding using measurements of photographic plates (Osterbrock, 1996). The plates, imaged some sixteen years apart, confirmed this expansion and indicated that, on the assumption of constant expansion, a nova-like outburst must have taken place about 600 years ago. After radio telescopes developed the ability to image sources, new observations of the R Aqr nebula revealed more structure. While taking spectroscopic measurements, Wallerstein and Greenstein (1980) discovered elongated jet-like structures extending northeast and southwest to 7 arcsec from the star. Solf and Ulrich (1985) carried out an extensive high spectral and spatial long-slit spectroscopic study that confirmed Hubble's findings from 1939. Better and deeper images in the radio, ultraviolet, infrared, X-ray, and optical spectral regions have been published over the years with better imaging technology showing structures in the nebula and jet that couldn't be seen previously.

The orbital period of this system has not been easy to determine. Merrill (1950) proposed a period of 27 years based on radial velocity measurements, but it was not supported by later observations. Willson et al. (1981) deduced an orbital period of 44 years from the long-term variation of the light curve. While this was not immediately accepted (Burgarella et al. (1992), Michalitsianos and Kafatos (1982), and Garnavich (1981)), the 44 year period appears now to be fairly widely accepted.

2.3 Models

A picture is worth a thousand words, especially when there is so much to see. Figure 2.3 shows the beautiful nebulosity surrounding the binary star hidden within. The whole system appears reddened because it is situated in a very dusty region of space, and its blue light is absorbed before reaching us. The jets, identified by Wallerstein and Greenstein (1980) and later resolved by Hollis et al. (1989), can be easily seen near the center of the image. As beautiful as this image is, it only tells us so much about the system. The two stars responsible for this reddish nebulosity are hidden within it and we can't clearly see how they interact. In

order to see beyond the haze, a better view is required.

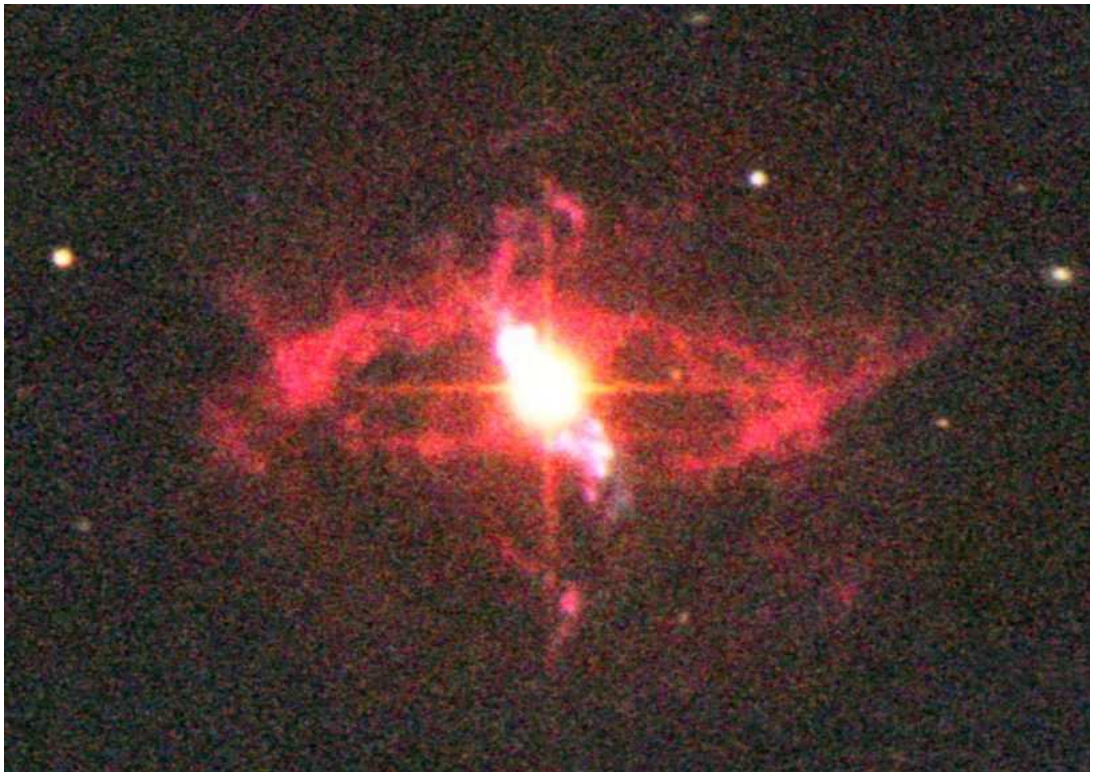

Figure 2.3: An image of the nebulosity surrounding R Aqr taken by David Malin at the Anglo-Australian Observatory.

It wasn't until 1973 the first radio images were taken to pierce through the haze. Gregory and Seaquist (1974) detected two radio sources near the center of the field. The Hubble Space Telescope took images of R Aqr in 1990 and revealed more of the central portion of the system. Two blurry globules can be seen in the center of the haze. Later on, these two sources were denoted by the titles C_1 (top) and C_2 (bottom). The structure of the two globules can be superposed very well on the HST images (See Figure 2.3). The collimated jet of R Aqr clearly appears in the F501N image (Paresce et al., 1991). The morphology of the feature C_2 is remarkably similar to a Herbig-Haro object. Herbig-Haro objects are small patches of nebulosity associated with newly-born stars, and are formed when gas ejected by young stars collides at speeds of several hundred kilometers per second with clouds of gas and dust nearby. Herbig-Haro objects are ubiquitous in star-forming regions, and several are often seen around

a single star, aligned along its rotational axis. With this idea in mind, the morphology of C_2 suggests that there is a collimated wind from the binary system, and that C_1 should contain both stars (Burgarella et al., 1992). Sadly, this bright globule $C_1$is the best we can see of the two stars.

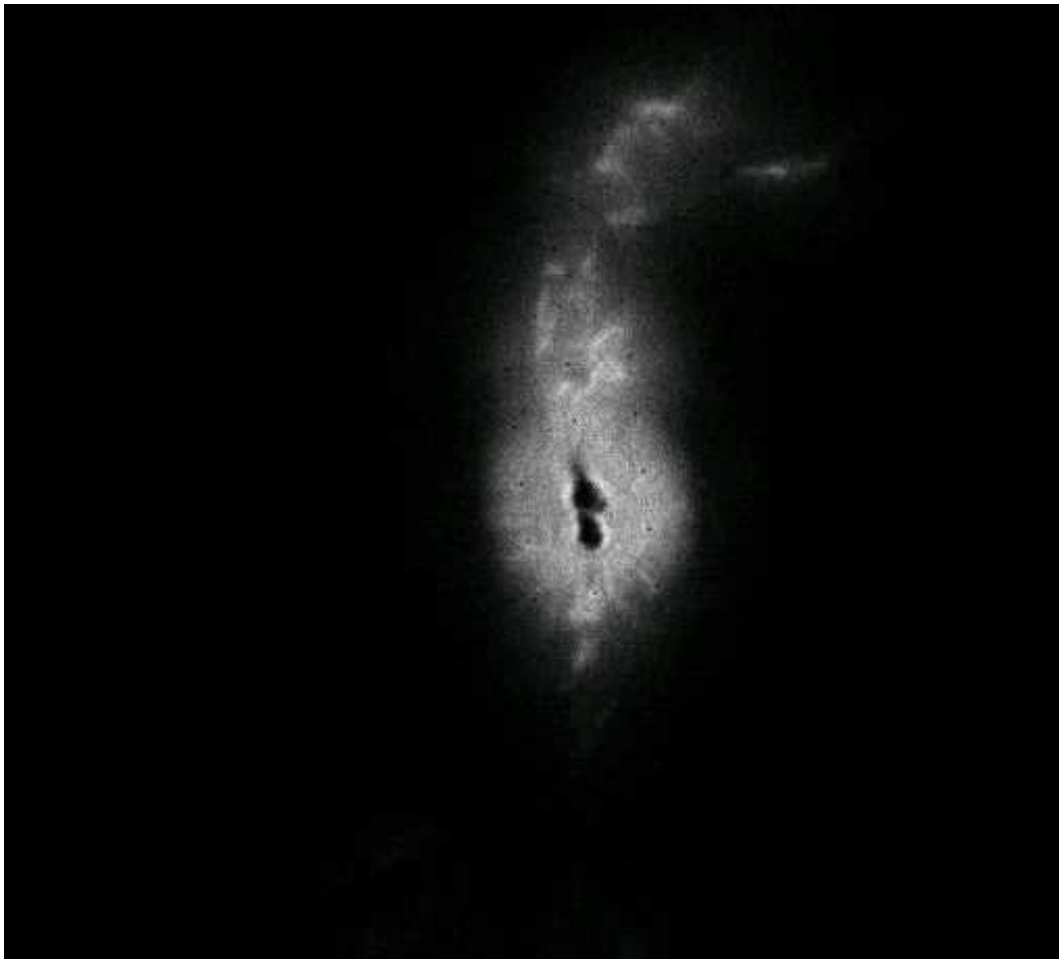

Figure 2.4: R Aqr from the HST Archives (Paresce et al., 1991).

How do these two stars interact? With so many interesting features apparent in this binary, there must be a cause. Since its period is long and we can't observe the two stars visually, we must rely on the tell-tale signs around the stars to constrain models that correspond to these measurements. Those signs are the jets, the nebula structure, the photoionization of the nebula, and the radio and X-ray emissions. These observations will be discussed in further detail in the next chapter.

The three most discussed types of models that have been continually used to portray R Aqr are the colliding winds model, the parcel model, and the accretion disk model. The *colliding winds model* involves the two winds coming from the stars and colliding. The first wind is from the cool giant and is massive, cool, and relatively slow. The second wind is from white dwarf and is fast, hot, and not very massive. The two collide, forming shock fronts that bend towards the star with the weaker wind. This results in a large spiral pattern and thus will be seen as successively farther points of brightness away from the central stars. The *parcel model* is based on the interaction of a hot isotropic stellar wind with a cooler cloud of gas. The hot wind creates a cavity of hot gas which escapes only through the direction of least resistance along the axis of rotation or the lines of magnetic field. The jets from the star appear in a tight spiral perpendicular to the plane of the stars. This also results in points of brightness away from the central stars. The *accretion model* involves an accretion disk of material that surrounds the white dwarf companion. In this paper, I will display all of these models in more detail and eliminate unlikely candidates based on research by others and the careful analysis of the data I have proposed here.

CHAPTER 3. Modern Research

R Aqr has been imaged and studied frequently in hopes to get a better understanding of this star. But how do astronomers study this star? Like many things in our daily lives, objects take on a new face when viewed in a different "light." For example, Venus looks like a cream colored sphere in optical light. With a radar imager, we see the land features on the planet. The same idea may be applied to R Aqr. In this chapter, we will discuss the different observations taken of R Aqr and what can be said about this binary. These observations include optical, infrared, radio, ultraviolet, X-ray, spectroscopic, and polarimetry.

Optical observations produce the beautiful pictures that everyone can enjoy. Pretty pictures are nice; however, astronomers can get more information by looking at different forms light coming from the star. Instead of relying on what their eyes can see, they process them in ways that reveal more than meets the eye. Optical wavelengths range from 3800 Å to 7900 Å (3.8×10^{-4} mm to 7.9×10^{-4} mm), and they can reveal visible features of the object. For example, color indicates temperature in stars; a bright blue star has a much greater temperature than a red star. Also, color in a nebula can be an indication of composition. Visible light is composed of all the colors of the rainbow. Each color represents a different wavelength in the optical range. When looking at spectra of stars, small bands of light are either present (emission spectra) or absent (absorption spectra). These present or absent lines indicate what elements are present.

In the range between 7900 Å and 1×10^6 Å (7.0×10^{-4} mm and 0.1 mm) lies infrared light. Infrared has a longer wavelength than visible light and it can travel through some kinds of material. For example, if you were to place your hands inside a garbage bag and look at your hands using infrared goggles, you would be able to see your hands through the bag! This

applies for nebulae and dust. Things that were once obscured by dust can be seen in a different light. In astronomy, the infrared range is broken down into near, mid, and far infrared: Far infrared covers the range between 1×10^6 Å to 1.3×10^5 Å (0.1 mm to 0.013 mm), and includes maser emission from circumstellar material. Mid-infrared covers the range between 1.3×10^5 Å to 3×10^4 Å (0.013 mm to 3×10^{-3} mm) where non-thermal radiation sources can be seen. Near infrared covers the range between 3×10^4 Å to 7000 Å (3×10^{-3} mm and 7×10^{-4} mm), including thermal radiation from bodies with $T < 100$ K (-276.9 °F). For the case of R Aqr, far and near infrared are more commonly used since R Aqr shows far infrared excess and hot material from the companion star.

Radio light ranges from 1×10^6 Å to 1×10^{10} Å (0.1 mm to 10 m) and, like infrared, is able to pierce through dust. Radio astronomy first started in the early 1930's. With the need for radio transmitting, bigger dishes were created to fit the need. Thanks to this advancement, radio astronomy was born when astronomers took radio dishes and scanned the sky.

In the range between 1200 Å to 3200 Å (1.2×10^{-4} mm to 3.2×10^{-4} mm) lies ultraviolet (UV) light. Around the 1920's balloons were launched to study the UV spectrum of the Sun and in the 1966 NASA launched the Orbiting Astronomical Observatory (OAO) to study UV from astronomical objects. We can not see UV from ground telescopes because UV photons get scattered or absorbed in the upper layers. In order for astronomers to observe ultraviolet light, they have to take their instruments above the atmosphere using upper atmosphere telescopes (balloon launches), and space based telescopes.

The X-ray spectrum covers the range 0.1 Å to 200 Å (1×10^{-8} mm to 2.0×10^{-5} mm), and lets us study things like jets, powerful energy sources, black holes, and cataclysmic variables (a star which irregularly increases in brightness by a large factor, then drops back down to a settled state. This brightness change is caused by matter from a near by star being accreted on to the smaller star). The study of astronomical objects at the highest energies of X-rays really began only in the early 1960's. Before then, we knew only that the Sun was an intense source in these wavebands. In fact, the discovery of the first cosmic X-ray source in 1962 came as a surprise. Scorpius X-1 was first X-ray source found while scanning for X-ray emission

coming from our moon (Giacconi et al., 1962)! As is true for ultraviolet light, our atmosphere absorbs or scatters X-ray photons.

Spectrometry is the technique used to assess the concentration or amount of a given element. As seen above, light come in many ranges. The absence or presence of certain wavelengths indicates something about the object we are looking at. In Figure 3.2, the individual lines that are present indicate certain elements that can be see in R Aqr. The instrument that performs such measurements is a spectrometer or spectrograph. This instrument contains a device that spreads the light a telescope receives and displays it in a vertical strip as seen in Figure 3.2. Most large telescopes have spectrometers, which are used either to determine the physical properties of astronomical objects or to measure their velocities from the Doppler shift of their spectral lines.

Last, but not least, we discuss the study called polarimetry, the study of polarization. Polarization is an important phenomenon in astronomy. Light is an electromagnetic wave and can be altered by a magnetic field or when scattering occurs. In the case of astronomy, light can travel through a medium which polarizes it and the light can appear different depending on the medium. Although the radiation of stars in not appreciably polarized at source, its scattering by interstellar dust or a magnetic field imposes polarization on starlight over long distances. With this understanding of the electromagnetic spectrum, what have astronomers seen in this R Aqr?

3.1 Optical

The first optical image of R Aqr was taken in 1921 by Carl Lampland using the Lowell Observatory. Lampland's image showed the wispy cloud of nebulosity around the star. He noted that there was not much in the brightness and structure of the nebula. From this, he concluded that perhaps the formation of the nebula is stable. However, he concluded that a deeper image was needed to better see and understand the star (Lampland, 1922).

As time went by, more powerful telescopes became available. With advancement in telescopes and detectors, more and more details of R Aqr could be seen. In 1988, the faint

nebulosity around R Aqr could be seen in much more detail than before with the advancement of more powerful telescopes. In 1993, the best image of R Aqr taken by a land based telescope was taken from the Anglo-Australian Observatory (Figure 2.3) by David Malin. Paresce et al. (1991) took things a step further using images from the Hubble Space Telescope (HST). With no atmosphere to distort the image and no worry about having the star set, the images using HST were taken for longer periods of time and they show much more clarity and detail (Figure 2.4).

While working beside Hubble with his research on the expanding universe, Baade took photometric images of RR Lyrae stars and other variables as well (Osterbrock, 1996). He analyzed images of R Aqr that were 16 years apart and confirmed Hubble's observation that the nebula around the stars was expanding and that, on the assumption of constant expansion, a nova-like outburst of the blue companion must have taken place about 600 years ago (Mattei and Allen, 1979).

Paresce et al. (1991) observed the inner R Aqr regions with a resolution better than $0.1''$ using HST. The inner region of the nebula was centered on the forbidden emission line [O III] 5007 Å. This emission line told Paresce that there was ionization occurring between these two stars and that oxygen was present. However, complications in the interpretation of the images arose. One such complication was due to saturation in the images. Sadly due to this saturation, absolute fluxes near the core were unreliable. However, Paresce did note that the outer structure is maintained and can give valuable indications on the morphology (Burgarella et al., 1992).

3.2 Infrared

In order to explain the far infrared excess found, Anandarao and Pottasch (1986) have suggested that two dust shells coexist in R Aquarii. The radius of the emitting inner shell is 4×10^{14} cm and the temperature is 800 ± 80 K. The outer shell has a radius of 9×10^{15} cm and a blackbody temperature of 87 ± 8 K. They note that the size of the large shell being approximately similar to the large halo partly due to their findings in the HST images. They

also note that spherical aberration may not be the only source producing the $\sim 2''$ disk visible in the HST images.

The temperature of the Mira itself was suggested to be about 2800 K (4580 °F) by Anandarao and Pottasch. Whitelock (1987) combined far-infrared data with her own JHKL near-infrared observations of several symbiotic stars. She found that among them, R Aqr is the symbiotic star which appears to have the nearest location to the regular Miras in both the $(J-K)_0$ vs. $(K-L)_0$ and the log (F_{25}/F_{12}) vs. log (F_{60}/F_{25}) diagrams, confirming the supposition that the red star in this system is a Mira.

3.3 Radio

The first radio image of R Aqr was taken by Gregory and Seaquist (1974). They were able to see two bright globules hidden in the nebulosity. Since then, a number of papers have been devoted to the radio-continuum mapping of R Aqr. The large scale structure has been studied by Hollis et al. (1986) but only recently have new VLA observations reached the high spatial resolution necessary to resolve the sub-arcsec structure. The radio continuum fluxes and spectral indices of the known important regions of the inner R Aqr nebula were culled from earlier papers dealing with radio-continuum observations. Its radio spectral index of $\alpha \sim 0.5$ argues for an optically thick thermal emission source. In his paper he assigns letters to the bright globules that are seen in Figure 3.1: C_1, C_2, A′, and A. C_1 is assumed to be the core of R Aqr that contains the binary system.

In radio astronomy, the spectral index of a radio source can hint at its physical properties. The spectral index is calculated from a power law dependence for flux. Sopka et al. (1982) have computed the resulting radio spectral index expected for a spherically symmetric steady mass loss to be $\alpha \sim 0.6$, very similar to the value found in C_1. Going farther out, feature C_2 was fully resolved by Hollis et al. (1986). In their 2 cm observations and using the 6 cm flux data from Kafatos et al. (1989), the radio spectral index $\alpha \sim -0.7$ shows the object to be non-thermal. Several other features, including S_1 and S_2, appear in the 2 cm contour plot (Figure 3.1). These features appear southeast of R Aqr and are probably optically thick and thermal sources. Hollis

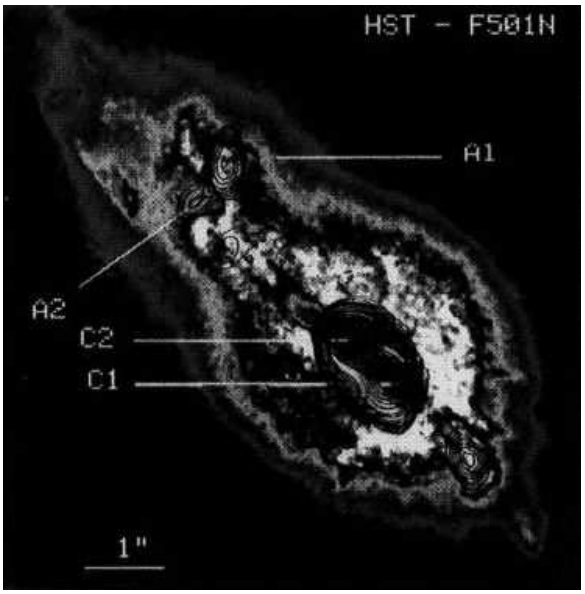

Figure 3.1: HST images of the inner $7''.7 \times 7''.7$ in the F 501 N filter (Kafatos et al., 1989).

et al. (1986) had already pointed out the difficulty of using low-resolution observations in trying to unveil the nature of distant symbiotic stars: only in a few systems is the spatial resolution good enough to allow the separation of some of the components. This also applies, although at another scale, to R Aqr. According to Kafatos, two features A appeared approximately at the same location in the 2 cm and 6 cm maps. These two features are probably different and their association may be only due to the low VLA resolution. The radio spectral index $\alpha = 0.3$ of the old feature A obtained from the 6 cm and 2 cm fluxes is intermediate between the optically thin ($\alpha \sim 0.1$) and optically thick ($\alpha \sim 2$) thermal source cases (Kafatos et al., 1989).

3.4 Ultraviolet

Kafatos et al. (1986) used the International Ultraviolet Explorer (IUE) for a four-year study of R Aqr. With the help of the high resolution VLA maps, they have separately observed the central H II region, the entire North East (NE) jet, and the extremity of the jet. The core of R Aqr shows a UV spectrum with low excitation O I, Fe II, and Mg II to moderate excitation [C III], [C IV], and [O III] emission lines (Michalitsianos and Kafatos, 1982). An interesting change in conditions of the jet was observed in 1985. High excitation N_V 1238 Å, 1242 Å

and He II 1640 Å emission lines appeared in the UV spectrum that were not apparent before. These lines are not cospatial with the continuum which is mainly emitted by feature B, but they are produced in feature A (Michalitsianos and Kafatos, 1982). Over 3.5 years, these lines showed a general increase in brightness 4 times that of normal. This probably reflects changes somewhere in the jet.

The temporal variation of UV emission lines on a time scale of 1.5 years observed by Kafatos is more obvious in the strong N V, C IV and He II lines and is therefore certainly due to a variation in emission mainly originating in feature A. The UV measurements imply an average electron temperature which is 18000 K for the central H II region and about 10000 K for feature B. The temperature of feature A apparently increased from 14000 K in May 1982 to about 19000 K in December 1983. Similarly, the electron densities deduced from the UV observations are $N_e \sim 3$–5×10^4 cm^{-3} for feature A, $N_e \sim 10^4$ cm^{-3} for feature B and $N_e \sim 10^6$ cm^{-3} in the central H II region (Burgarella et al., 1992).

3.5 X-ray

For R Aqr, the objects that are continually studied in X-ray are the NE and SW jets extending from the binary (see Figure 2.3). In the image, two bright beams extend NE and SW from the central point.

EXOSAT observations by Viotti et al. (1987) led to an unambiguous X-ray detection of R Aqr. Viotti showed that the source is probably soft and almost unreddened with a 0.2–1 keV luminosity of 0.8–1.0×10^{30} erg s^{-1}. This is a relatively low emission flux compared to other symbiotic stars. Two interpretations have been advanced: (1) a model consisting of a central source photoionizing the circumstellar material, and (2) a model where the emission is associated with shocks produced in the interaction between ejected and circumstellar matter. Photoionization could eventually play a role in this latter scenario. Unfortunately, the X-ray measurements are not sufficiently constraining to eliminate one of these models. However, the X-ray elongated shape of R Aqr in the NE-SW direction may suggest that the X-ray emission originates in the NE jet.

Hollis et al. (1989) carried out IUE observations of the NE jet of R Aqr in June and in December of the same year they observed the SW jet. From this data, they deduced that the NE and SW jets have densities $N_e \sim 10^3$–10^4 cm^{-3} and roughly similar excitation conditions. Although they found indications for a slightly higher density and lower temperature in the SW jet, their results were in good agreement with the NE jet, apart from the high ionization lines that seem to have increased in intensity.

3.6 Spectrometry

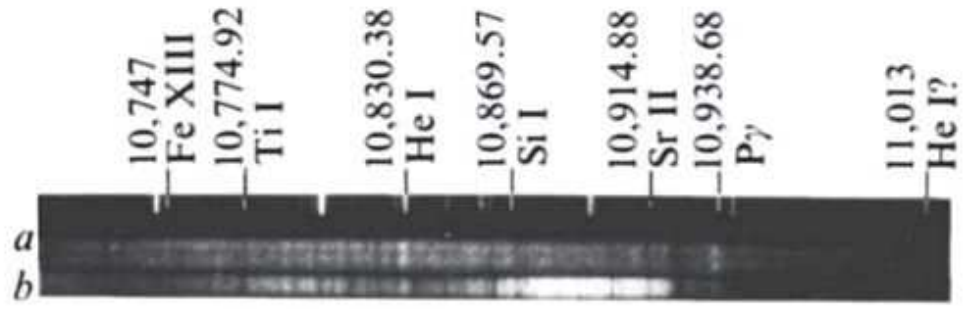

Figure 3.2: Two image tube spectrograms of R Aquarii taken by Zirin (1976). **a**, September 1968, phase 0.01 (maximum light); **b**, July 1970, phase 0.79, with identified lines and wavelengths marked.

The first spectral observation was taken by Merrill (1919) from the Mount Wilson Observatory. Poor observing conditions prevented satisfactory observations at Mount Wilson in the short time that remained after maximum before the object was lost in the western sky. However, he was able to classify R Aqr as Md type star[1] since it showed lines at 4102 Å, 4340 Å, 4364 Å, 4470 Å, 4571 Å, 4861 Å, 4959 Å, 5007 Å. These lines correspond to the elements of Hydrogen (4102 Å, 4340 Å, 4861 Å), Helium (4470 Å), and Magnesium (4571 Å). In 1950, Merrill was able to classify the star more clearly as a Me star using more detailed spectroscopic analysis he took in 1936–1949 (Merrill, 1950). The "e" stands for emission; Mira variables typically are of Me, Se or Ce type.

[1]The Md classification does not appear in the more recent literature.

As the years went by and observations of R Aqr became available in other wavelengths, spectrometry in those bands was also studied. Zirin (1976) detected radio emission from the R Aqr in 1970 (Figure 3.2). They were in the middle of a He I = 10,830 Å spectral survey at the time. In the course of reducing plates of this star made in 1970 and 1971, he found the emission line of the forbidden coronal transition of Fe XIII at 10,747 Å. Shore et al. (1992) found a number of emission lines present at the jet offset position, particularly N V 1240 Å, C II 1335 Å, C IV 1550 Å, He II 1640 Å, [O III] 1665 Å, [N III] 1750 Å, [C III] 1906 Å, [C II] 2325 Å, [O II] 2470 Å and Mg II 2800 Å. For N V and C IV in particular, the spatial position of the corresponding emission component is not centered on the UV continuum, but is displaced relative to the UV continuum. They note that two lines, however, Si II 1265 Å and O I 1300 Å do not exhibit extended or displaced structure, and are essentially cospatial with the UV continuum. The presence of the highest excitation line emission in the knots which comprise the jet is consistent with thermal induced emission from shocks that locally excite the gas. In total, R Aqr shows signs of Hydrogen, Helium, Magnesium, Nitrogen, Oxygen, Iron, Carbon, and Silicon.

3.7 Polarimetry

For two decades, it has been known that the radiation from R Aqr is polarized (Shakovskoi, 1969; Aspin and Schwarz, 1988). The polarimetric observations of Schwarz indicate a wavelength dependence of the polarization in position angle ($\sim 120^\circ$ in UV and highly variable in visible and IR), percentage of polarization and time. UV light has been sometimes highly polarized up to 19%. However, Nikitin and Khudyakova's R and I measurements shows that polarization rose to $\sim 10\%$ in 1976 and decreased again to low values the following year (Nikitin and Khudyakova, 1979). One possibility is that the increases in the UV, R and I could have been caused by the same phenomenon that produced the appearance of a new NE elongated feature in the inner nebulosity of R Aqr between 1970 and 1977 and the eclipse deduced by Willson et al. (1981).

The last *UBVRI* polarimetric observations by Deshpande et al. (1987) confirmed the high

UV polarization. This intrinsic variation in polarization implies changes in the scattering geometry and/or efficiency in the R Aqr system and suggests that at least two mechanisms are at work here: one in the UV and the other one in the visible. The steady position angle around 120° in the UV and the much more variable position angle in the visible can be explained if some matter orbits around the hot component of the binary system. UV photons can escape only in a direction perpendicular to the matter orbiting around the hot star, in the direction of the jet (p.a. = 29°), which scatters the polarized light perpendicularly to the direction of the jet. On the other hand, visible photons are preferentially scattered in a shell surrounding the Mira and the resulting polarization angle is due to changes in the nebulosity.

Over the past 50 years, R Aqr has been observed in all parts of the electromagnetic spectrum in hopes of better understanding this Mira binary. Each wavelength provides new information and gives us a different view of R Aqr. With each new observation, the mystery surrounding this star is slowly being unraveled. The next step is to apply models and comparisons of well-known systems to this binary; this will be the purpose of Chapter 6.

CHAPTER 4. The R Aqr Database

When it comes to R Aqr, knowledge does not come a priori. Much of the knowledge of R Aqr has come from several years of observation, research, and analysis. The best place to start research is through a database where a great amount of information on a certain/multiple topic(s) can be found. However, if the topic is covered over many years, the amount of information may be daunting. In fact, there are already 575 papers on NASA's Astrophysical Database System (ADS) that deal with R Aqr, and this number is still growing. So where do you start? If you are looking for some specific information about the system, this is a rather formidable number of papers to check. My initial task was to sift through all those papers available, gain knowledge on the study of R Aqr, and to create an easy access database to store and reference all the papers I obtained.

4.1 Selection

The initial search began using ADS. Using the search engine, I looked up any paper that mentioned R Aqr or R Aquarii in any form. The earliest paper dates back as far as 1919 and a total of 574 papers were listed. However, not all papers were available for my use through ADS. Some only had abstracts available. Others could only be accessed through a website outside of ADS that required membership. Finally, it was necessary to set a final cut off date. We chose October 2008 to keep things simple. With this cut off, the database contains 177 papers.

4.2 Database Creation

The database was created as an easy means of referencing the papers I had collected. The basic design of the database included categorizing papers by Author, Category, Year, and Journal so that the viewer only needs to know that particular piece of information to find the paper they are looking for. I used Microsoft FrontPage to create .html files with hyperlinks to each topic. I chose FrontPage as the platform for the database since it was a program I was more accustomed to, and I could easily make it accessible to anyone via the internet. Figures 4.1 through 4.3 are images of the database.

I first created the main homepage and links to other pages associated to the database. They were empty at first, but this would soon be remedied. Next, sifted through all of the papers to sort them into the respected subcategories: Interferometry, Infrared, Jets, Models, Nebulosity, Optical, Photometric, Polarimetry, Radio, Spectroscopy, Ultraviolet, and X-ray. Each subcategory represents the topic or type of observations described in a particular paper. These subcategories were placed as links on the Category page, and individual pages were created for each. After categorization, I listed the papers by title (alphabetically), authors, and ADS quick reference number.

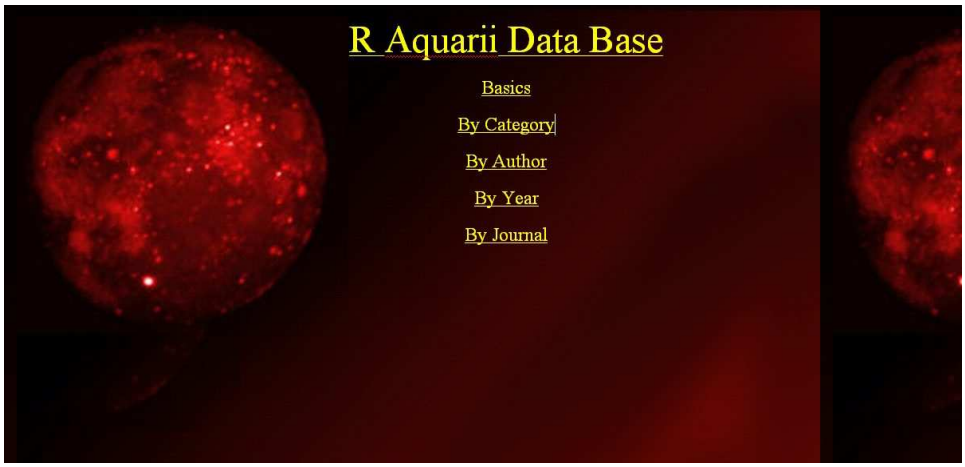

Figure 4.1: The main page for the R Aquarii Database.

Next came the long the process of reading the papers. I started reading papers by sub-

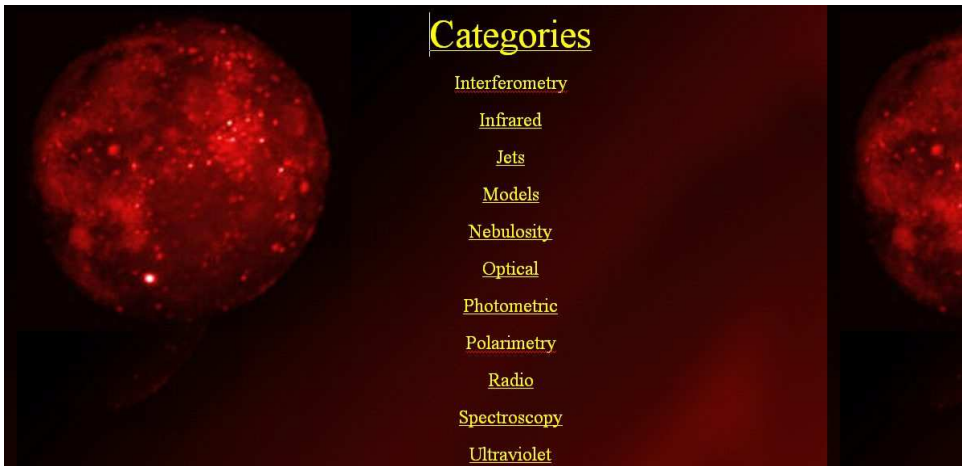

Figure 4.2: The Category page within the R Aquarii Database. Each category listed has a hyperlink to a page listing the papers pertaining to that specific category.

category to keep a consistent line of thinking as I would read through the material. After reading a single paper, I would create a personal summary of that paper. After all the papers in a subcategory, I would create a links on the subcategory page that would link users to the original paper, a copy of the paper's abstract, and my personal summary for each paper. Some papers prior to 1940 would often not have an abstract. To simplify this, I would create a personal abstract for the paper. Two papers, Graff (1920) and Solf and Ulrich (1983), I posted a link to translations by Martin Schroedter since the papers were in German.

In the midst of reading, I came across papers from well known astronomers. These include Hubble, Baade, Shapley, and Merrill. These authors were known for their other contributions to astronomy, but still did research on R Aqr. As mentioned in §2.2, Hubble in 1939 detected the expansion of the nebula using differences between different images taken 17 years apart. After Hubble's departure during the war, Walter Baade confirmed Hubble's finding using measurements of photographic plates. Shapley posted a request for observation of R Aqr in 1927. Merrill was a leading astronomer in infrared research and identified lines of technetium in R Andromedae and other S-type stars. I also noticed certain years where nothing would be published. Figure 4.4 shows a chart of the years of publication and the number of papers. It was after 1979 the number of papers published greatly increased with the largest amount of

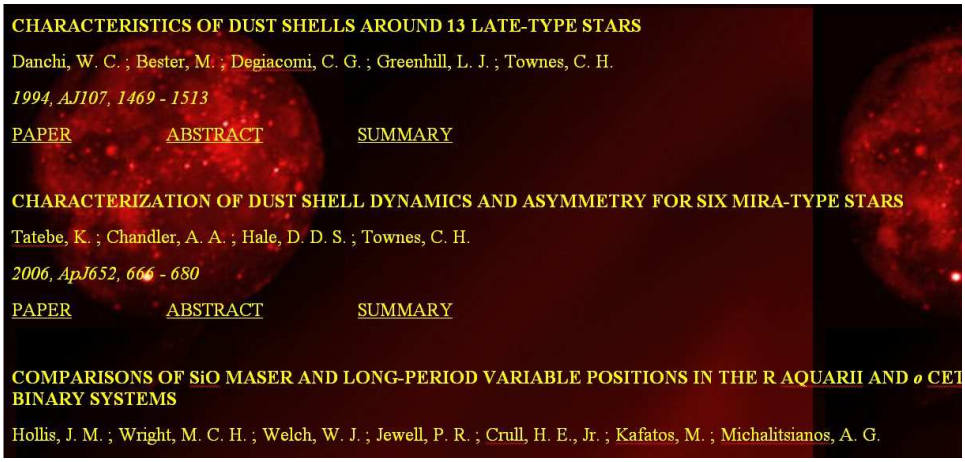

Figure 4.3: An example of the listing of papers in a category. This page contains papers pertaining to interferometry.

publications around 1992, the year with the first HST images of R Aqr.

After all the subcategories were completed, the next step was to post the information of each individual paper on their respected year and author page. One paper alone could appear 3 or more times within the database given the author(s), year, and categories covered in the paper. Figure 4.5 shows the number of papers per category.

Upon completion of the database, my next step was to publish it online. Sadly, my first attempt to publish the database failed due to the large size of the database. Since each of the papers was much larger in size, the total database was over 5 GB! The maximum that Iowa State allows for publication is 1 GB. In order to greatly reduce this amount, I created a hyperlink to the individual papers on ADS. Not only did this step reduce the size to 25MB, but it complied with copyright laws since you need a membership in order to access some of the papers through ADS. The database can be accessed through my personal website, `http://www.public.iastate.edu/ãstro01/homepage.html` under R Aquarii Database.

4.3 Paper Comparison

While I was reading through the numerous papers, I began to notice certain traits and styles between the papers. These styles I have labeled as Letter Format, Single Column Format, and

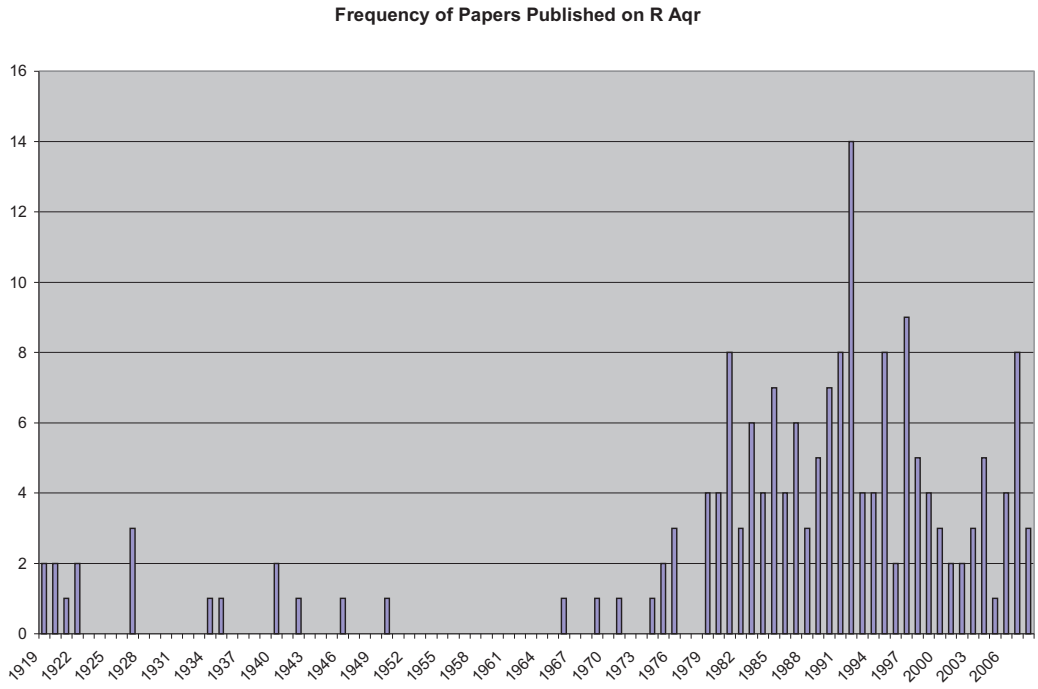

Figure 4.4: Bar graph showing the number of papers published in a given year.

Double Column Format. I found this to be interesting since it shows a transition of writing preferences and journal requirements over the many years of scientific writing. I also noticed that scientific papers can fall into three categories Pure Observational Format, Observational with Models Format, and Theoretical Format.

Single Column Format describes papers that appear in one straight column. Their margins are often 16.5 cm with very little to no break in them (except for the occasional paragraph indent). This style was common prior to the 1970's. Before the age of personal computers and the internet, everything had to be typed up on a typewriter and sent off through the mail for distribution. The information would often take months to be distributed evenly to the scientific community.

Letter Format describes papers that range from 1 paragraph to one page in length. These papers were meant to inform their audience or the journal what they have discovered without going into much detail. Many papers that follow this format rarely had references and were

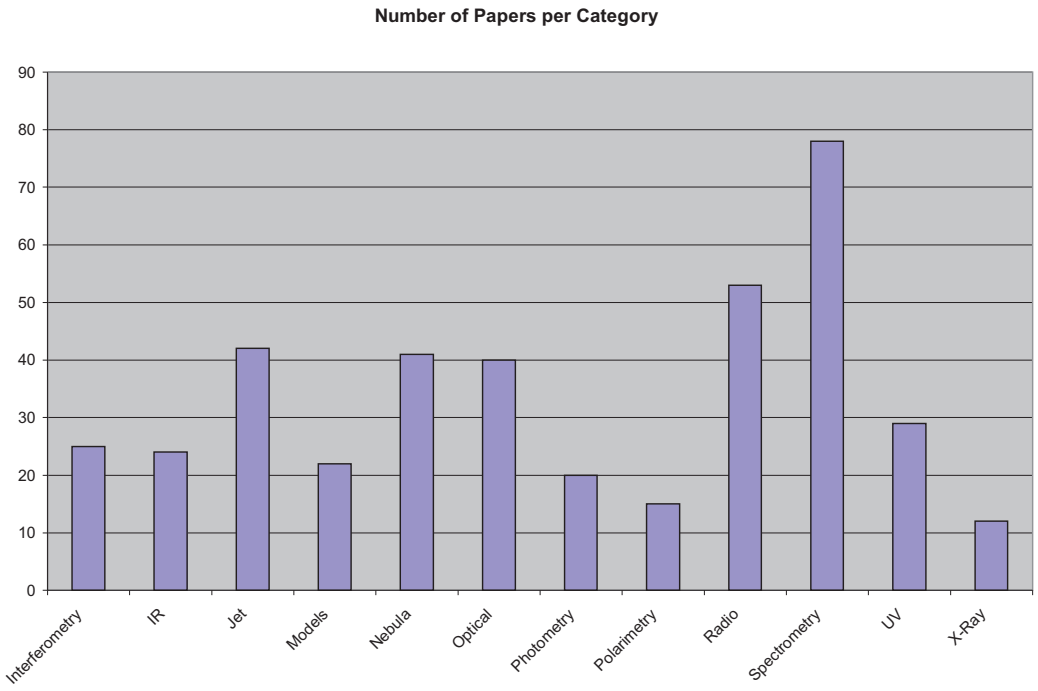

Figure 4.5: Bar graph showing the number of papers pertaining to each category. Some papers often pertain to more than one category.

often written by one person. All Letter Format papers were in Single Column Format.

Double Column Format describes papers that are broken into two columns of text on one page. The margins or each column is 8.1 cm, which is half that of Single Column Format. This was done to reduce the amount of sheets covered in one scientific paper. This style started in the 1970's and is commonly used today.

Pure Observational Format describes papers that just display the results of their research and observations. Often long and filled with tables, these papers describe the process they went through to get their results. If this is not combined with theory, they usually don't conclude with anything and just state the facts. Pure Observational Format papers were common from the 1940's through the 1970's, and sometimes have references, but not very many.

Theoretical Format describes papers that models that are produced to describe the system. These are one of most practical type of scientific papers since you see their step by step process they made to come to their conclusion. These types of papers use physical concepts and

equations to theoretically describe the system. Often these types of papers produce a model which is then validated by observations made by others. Theoretical papers describe physical models produced via data or computations. Prior to the computer age, simple and descriptive models were the norm. One example of a theoretical paper is Hollis and Koupelis (2000), on the *Lorentz Force-Driven Parcel Model*.

Observational with Models Format describes papers that focus on the observations the authors made. These papers differ from the Pure Observational Format in two ways: First, they propose or discuss some physical model for the system, and second, they are more likely to refer to observations made by other observers. The models mentioned in the paper aren't discussed in great detail, but their references guide the reader to the original theoretical paper that does. Two such models are simple models (basic idea or explanation), and descriptive models (describes the system based from observations). Two examples of Observational with Models Format papers are Burgarella et al. (1992), *A Model for R Aqr from HST*, and Gray et al. (1998) on *Testing the 'Clump' Model of SiO Maser Emission*.

All of these types of papers are seen within the database. Figure 4.6 shows a histogram of the number of papers in each paper comparison category over the multitude of years R Aqr has been studied. I decided to make three different bars per category to indicate "cut offs." These "cut offs" show the dramatic transitions of certain categories over the years. It is important to note that a paper can exist in more than one format, For example, Merrill (1919) lies in both the Single Column Format and Pure Observational Format. It is interesting to see the transition from Single Format, Letter Format, and Pure Observational to Double Format, Observational with Models Format, and Theoretical Format.

With this database at my fingertips, I was able to reference papers needed for my research on the different models used for R Aqr and how they compare with one another.

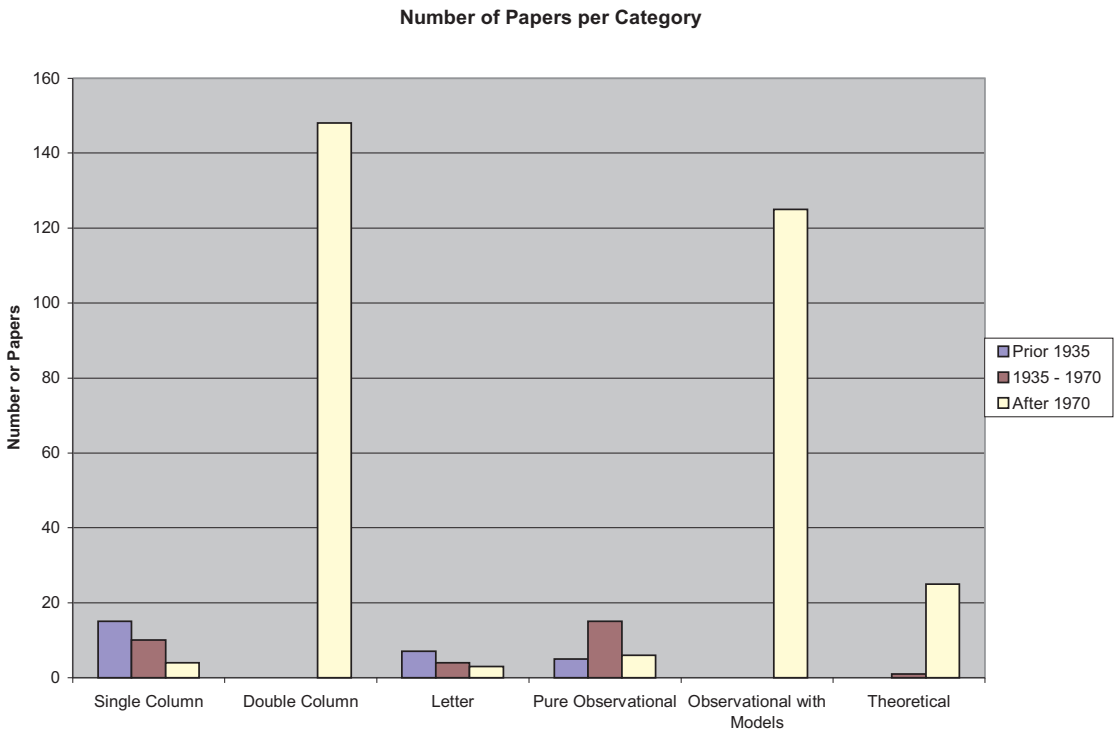

Figure 4.6: A histogram of the number of papers per paper comparison category. The legend indicates the cut offs.

CHAPTER 5. Image Analysis

In §2.3, three models of the jets of R Aqr were introduced. Here, I took the first step to put those models to the test by analyzing images from HST. These images are some of the best optical images taken and have shown great detail of the jets.

5.1 Image Selection

Before any research could be done, images were needed to be obtained. My initial goal was to use as many images as were available to compare and contrast different measurements from different telescopes. Using the Space Telescope Science Institute (STScI) homepage, I was able to retrieve several images taken by the following telescopes: The Extreme Ultraviolet Explorer (EUVE), HST, The Galaxy Evolution Explorer (GALEX), The Spitzer Space Telescope (Spitzer), The Infrared Astronomical Satellite (IRAS), Near Infrared Camera and Multi Object Spectrometer (NICMOS), Two-Micron All Sky Survey (2MASS), and The X-Ray Multi Mirror Telescope (XMM).

After retrieving them from their archive, I used a program known as KARMA using the kvis (k "view") package on a Linux machine. After careful study, I began to realize that some of the images could not be used in my research and were excluded. The GALEX (Figures 5.1 and 5.2), IRAS (Figures 5.3 and 5.4), Spitzer (Figures 5.5 and 5.6), and XMM (Figures 5.7 and 5.8) images showed a simple heavilyGALEX pixellated star. These images were not useful for analysis due to the small resolution of the telescopes. The NICMOS (Figure 5.9) and EUVE (Figure 5.10) images were spectral line images rather than object images. With all of these images excluded, the only images I could work with were from 2MASS and HST.

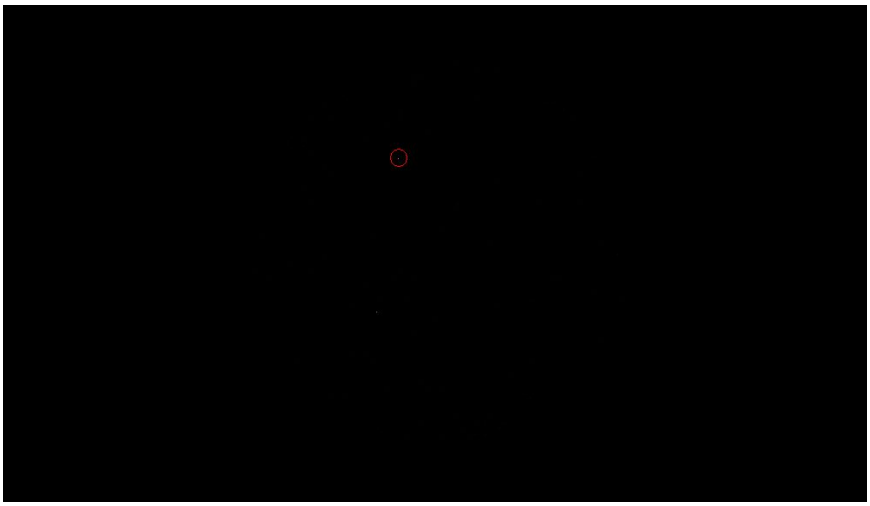

Figure 5.1: R Aqr taken in by GALEX in 2003.

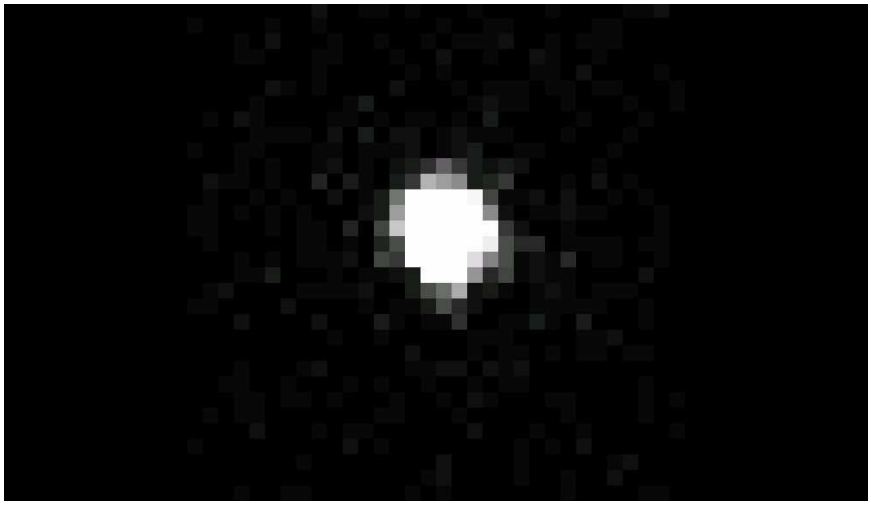

Figure 5.2: A zoomed in view of Figure 5.1.

Figure 5.3: Image of R Aqr taken by IRAS in 1990.

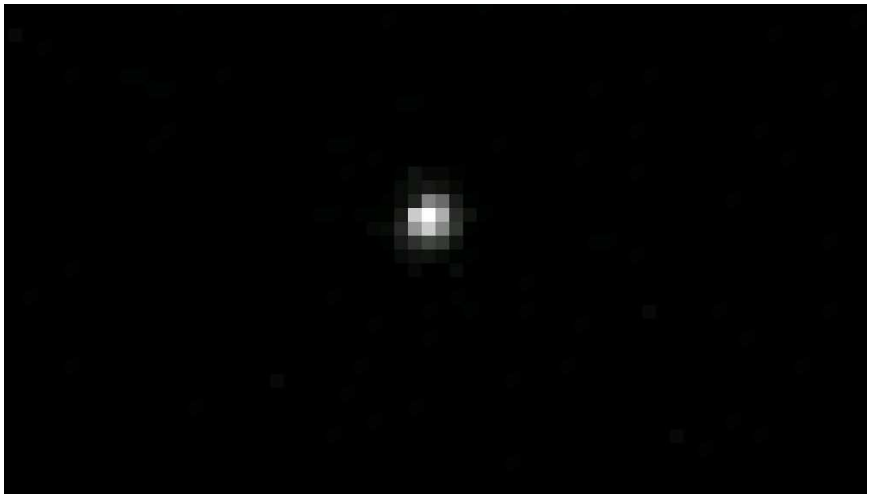

Figure 5.4: A zoomed in view of Figure 5.3.

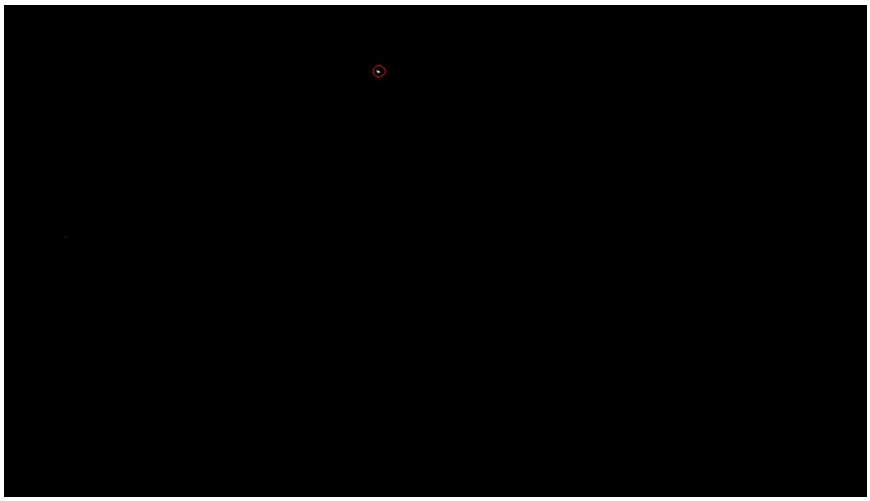

Figure 5.5: Image of R Aqr taken by Spitzer in 2006.

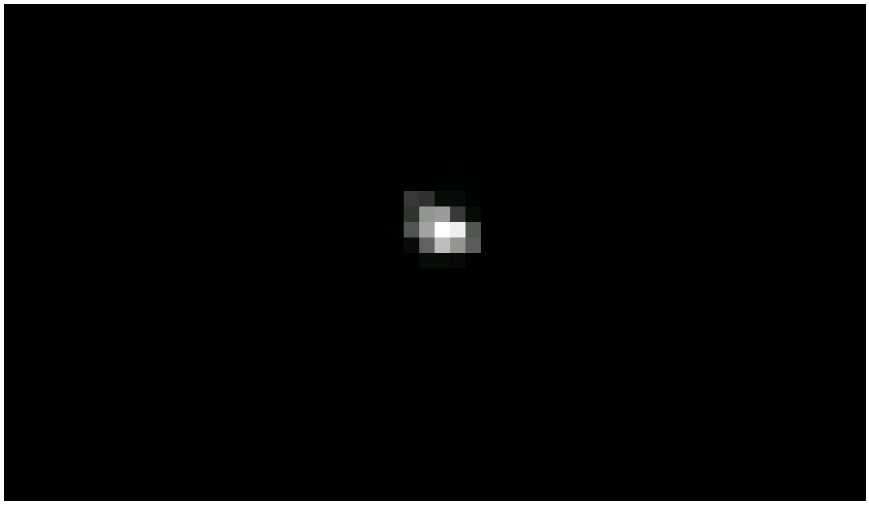

Figure 5.6: A zoomed in view of Figure 5.5.

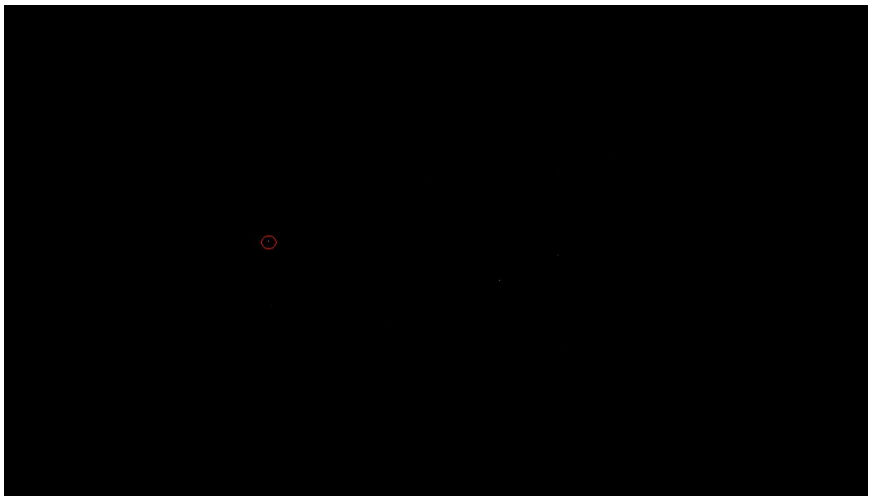

Figure 5.7: Image of R Aqr taken by XMM in 1995.

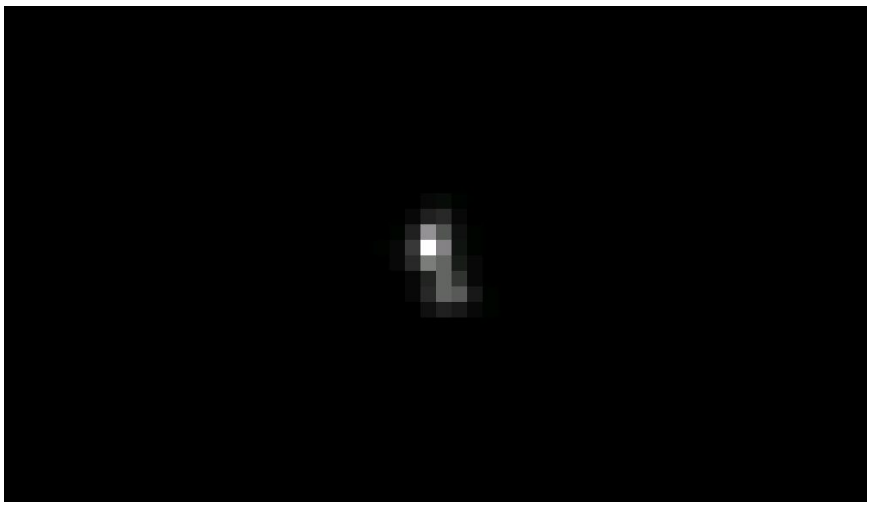

Figure 5.8: A zoomed in view of Figure 5.7.

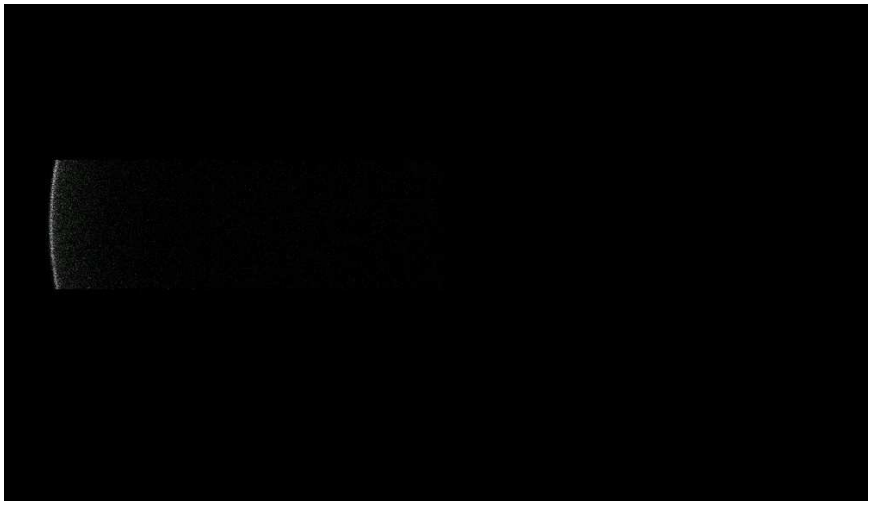

Figure 5.9: Image taken by EUVE in 1993. Signal strengths at certain positions were uniform vertically indicating this was a spectral image.

Figure 5.10: Spectral lines taken by NICMOS in 1998.

5.2 2MASS Reduction and Analysis

2 MASS is a collaborative effort of two 1.3 m telescopes to image the entire sky in the 2 m waveband. With these two telescopes, the resolution of these combined telescopes is around .3 arcsec. I first took on the 2MASS images which were separated into H, J, and K images. Rather than combining them to make a color image, I analyzed them separately since each H, J, and K image was a different band in infrared (H = 1.6 μm, J = 1.2 μm, and K = 2.2 μm) and to see if they differ from one another. After making several images and plotting several contours, I came up with a few good images that show some interesting features. The count range of the H band images were -65 to 11686. The count range of the J band images were -281 to 11271. The count range of the K band images were -402 to 11195 counts. The central source, RA: $23^{\mathrm{h}}43^{\mathrm{m}}49.39^{\mathrm{s}}$ and Dec: $-15°17'4.97''$, was removed from each of the images due to over exposure already present and is the cause for the negative number in photon counts. All of the images showed a few similar features; near the bottom of the screen at RA: $23^{\mathrm{h}}43^{\mathrm{m}}49.33^{\mathrm{s}}$ and Dec: $-15°18'25.97''$ lies a small circular source, there are four spikes stretching out from the center due to over exposure, and the circular pattern is lopsided toward the right (Figures 5.11 through 5.13).

The next step was to create contours of each of the images to find different bright sources and see the general flow of light (Figures 5.14 through 5.17). The final scaling for each of the images was done linearly every 100 counts to show where the prominent peaks lie. The small patch near the bottom of each image showed more greatly. However, after further investigation this patch is actually a natural error in the telescope do to internal reflection and was excluded in Figure 5.15. In Figure 5.16, this patch and the spikes are removed to see if there are any interesting features hidden within the glow. The right side oblongation can be clearly seen and is not an error from the telescope. Zooming 10 times into the center we start to reach the limit of the telescope (Figure 5.17). However, just outside the removed central source we find several bright points that could prove to be something. Since this is close to limit of the telescope, a reliable and low error analysis can't be done.

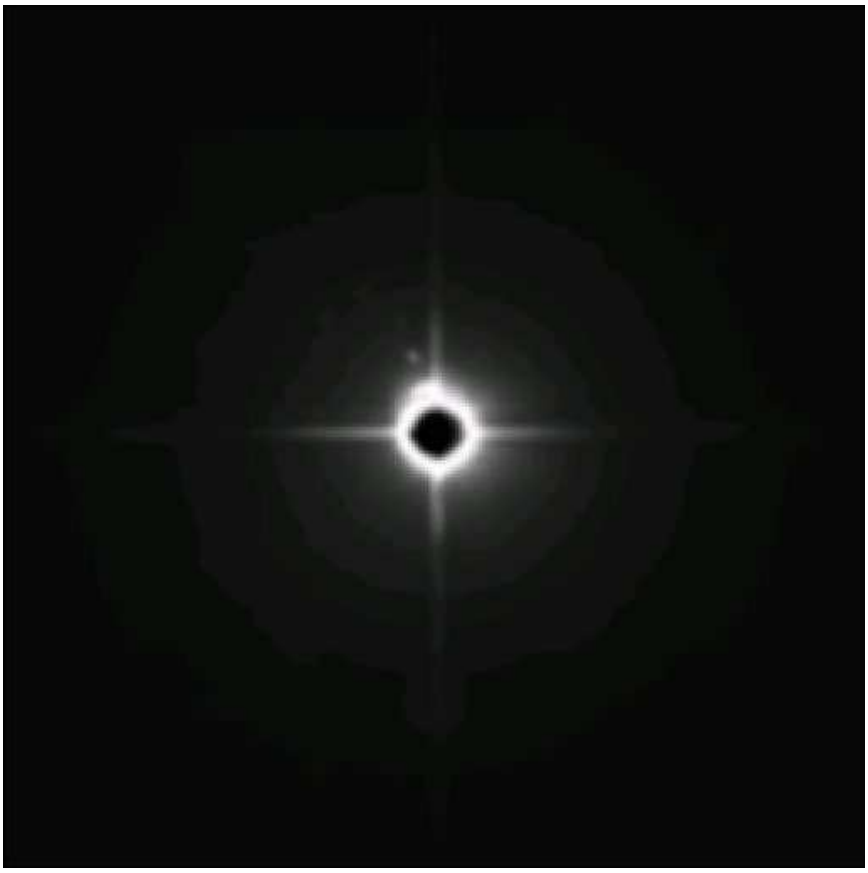

Figure 5.11: Image of R Aqr taken by 2MASS using the J filter in 2003.

5.3 HST Reduction and Analysis

This led me to images taken by HST, which have proven to be more reliable in showing greater detail and are comparable to David Malin's image (Figure 5.18). With a 2.4 m primary mirror, it would result in a better resolution than the 2MASS images (0.05 arcsec). Using STSCI's website, I was able to download several images from HST dating 1992. After several hours of analysis, a professor mentioned that these images contained spherical aberration from the uncorrected mirrors on HST. Any image dating prior to 1993 (which is when COSTAR was placed on the telescope) would show this aberration (Figure 5.19). I was then guided to a C based program, known as Tiny Tim, that would remove the aberration using test patterns provided through HST. After countless hours of trying to code in a language I am not familiar with, I could not get a reasonable image to analyze. Figure 5.20 shows my best attempt in

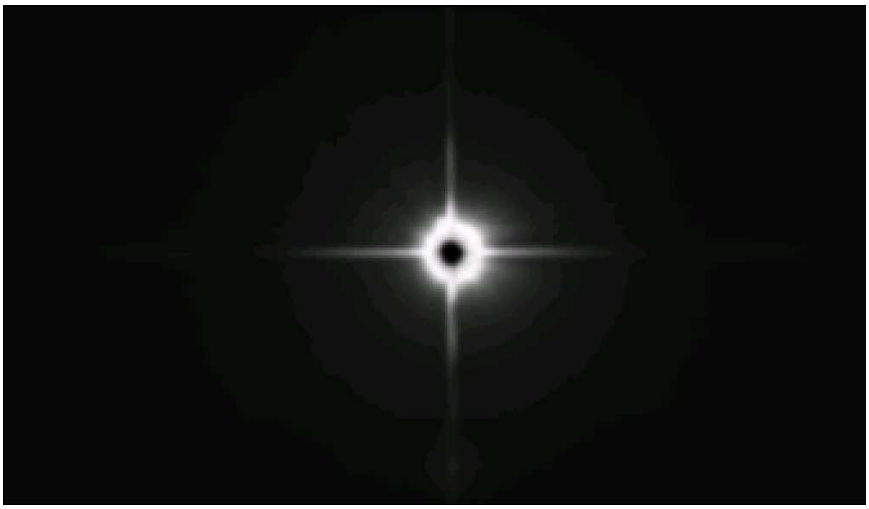

Figure 5.12: Image of R Aqr taken by 2MASS using the H filter in 2003.

reducing the image. After asking aid from a friend and mentor, Chris Anderson, he guided me to Eddie Bergeron, who currently works with HST. Mr. Bergeron gave me a link to a few images of R Aqr that were restored and some taken post COSTAR as seen in Figure 5.21. The images were great and the source counts were indeed greater than my Tiny Tim images.

With this new set of data, I created contours to show the location of peaks and their maximum height. Figures 5.23 through 5.25 are examples of the multiple contours created to show an image with the bright sources clearly visible. The most top bright source is called A$'$, which is part of the NE jet. In the center lie the four sources C1, C1a+b, C1c, and C2. C1c is thought to be the two stars. Lying just north of C1c is another source called C1 since it at first glance it appears to be apart of C1c. However, Gregory and Seaquist (1974) were able to detect a separate radio source coming from position. The bottom source is called C2 which is part of the SW jet. The farthest source is called A1 which is near the end of the SW jet (Figure 5.22). Each HST image is taken at the same exposure. After analyzing the images, I tabulated the location of the bright sources and the count of each source (Table 5.1).

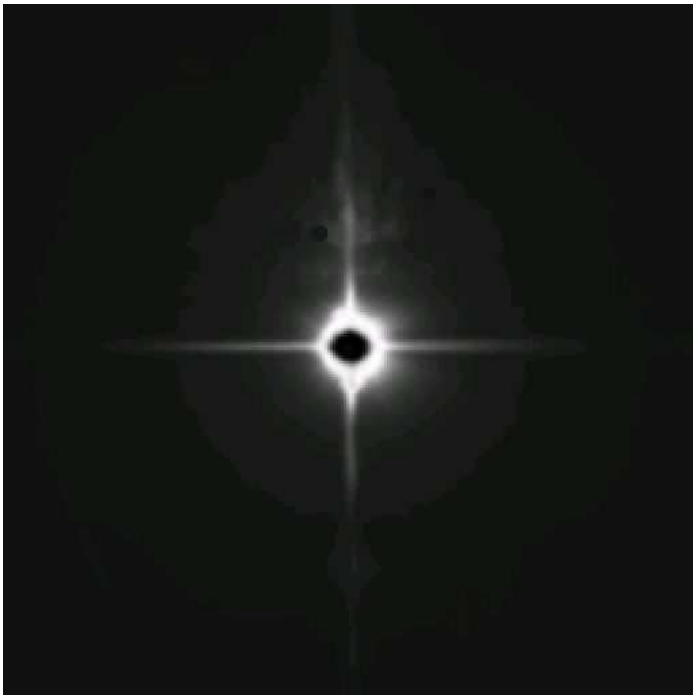

Figure 5.13: Image of R Aqr taken by 2MASS using the K filter in 2003.

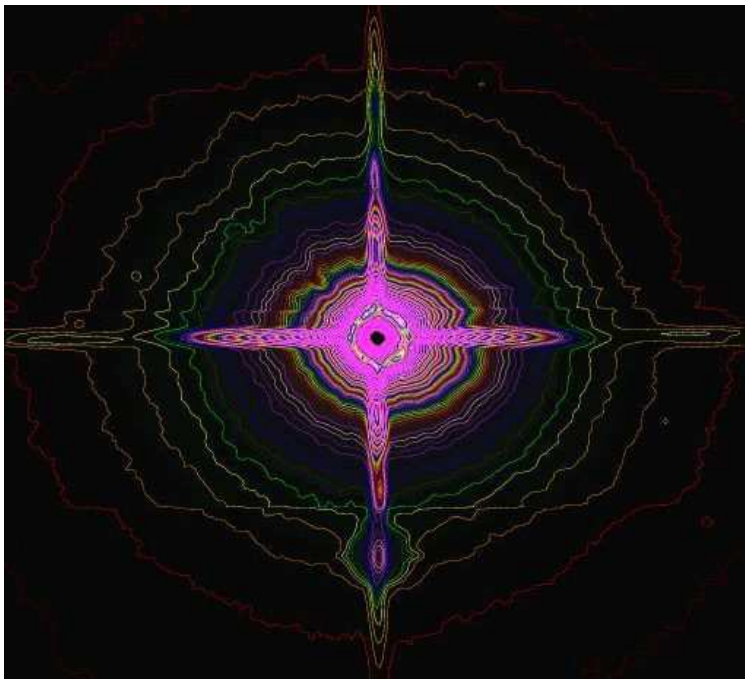

Figure 5.14: 2MASS H filter with contours every 100 counts.

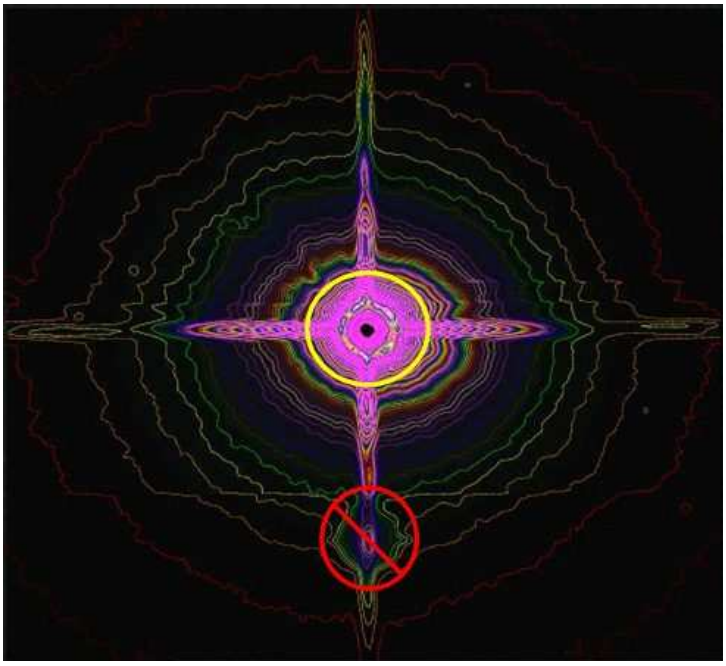

Figure 5.15: 2MASS H filter with contours every 100 counts. The red circle with the line through it indicates where the false source due to internal reflection is located. The yellow circle is for a reference to show the oblongation on the right side of the source.

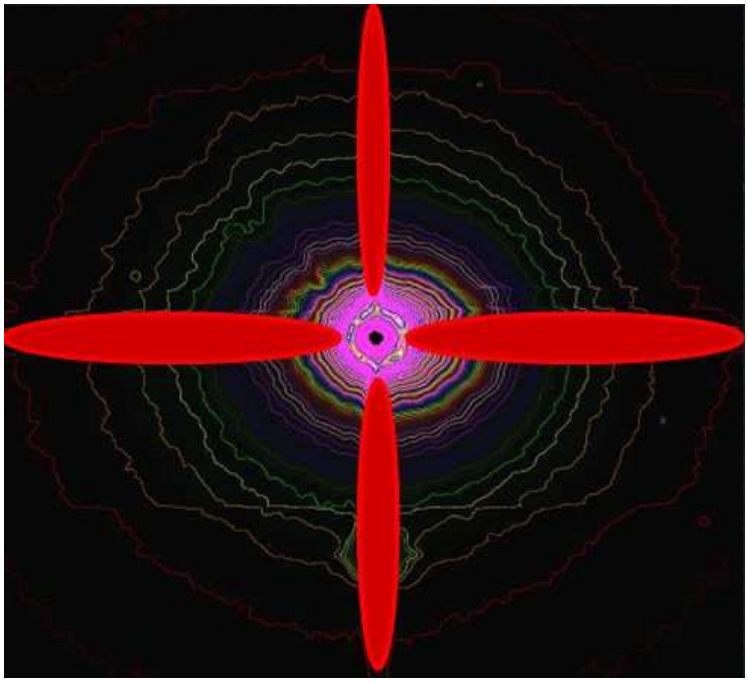

Figure 5.16: 2MASS H filter with contours every 100 counts. The star spikes are removed to show the uneven nature of the image.

Figure 5.17: The uplcose image of the 2MASS H filter. The red circles indicate the sources that are near the star. However, this is getting close to the 3 arcmin limit of the telescope

Figure 5.18: A composite picture of the AAO image overlapping HST F253M image.

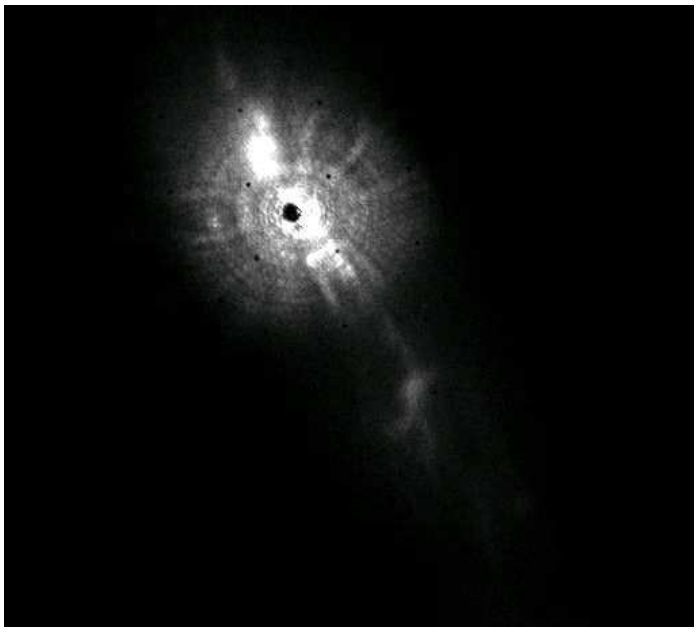

Figure 5.19: 1992 HST POL0 F501N image of R Aqr, prior to COSTAR. The "spider-like" structure is due to spherical aberration from HST.

Figure 5.20: My best attempt using the program Tiny Tim in hopes to remove the spherical aberration from Figure 5.19.

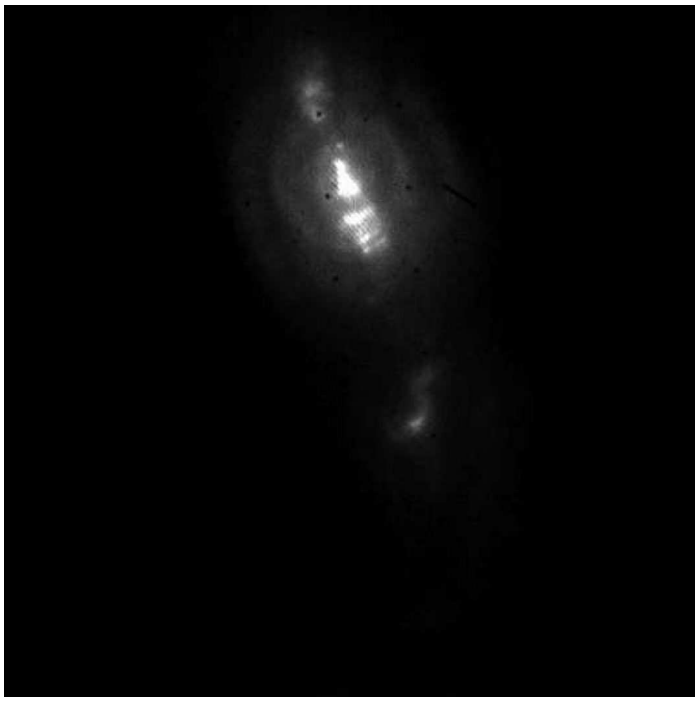

Figure 5.21: 1993 HST F253M, post COSTAR.

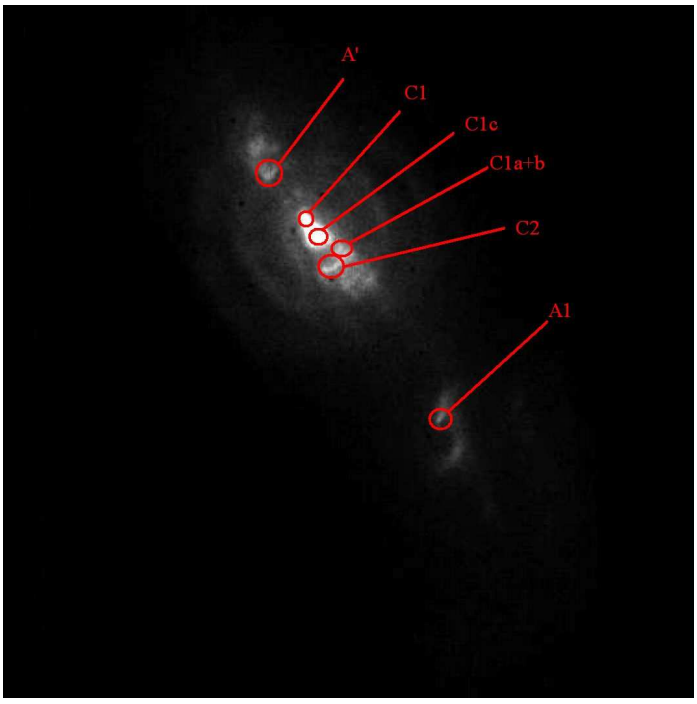

Figure 5.22: Locations of the brightest sources on the 1992 HST F278M image.

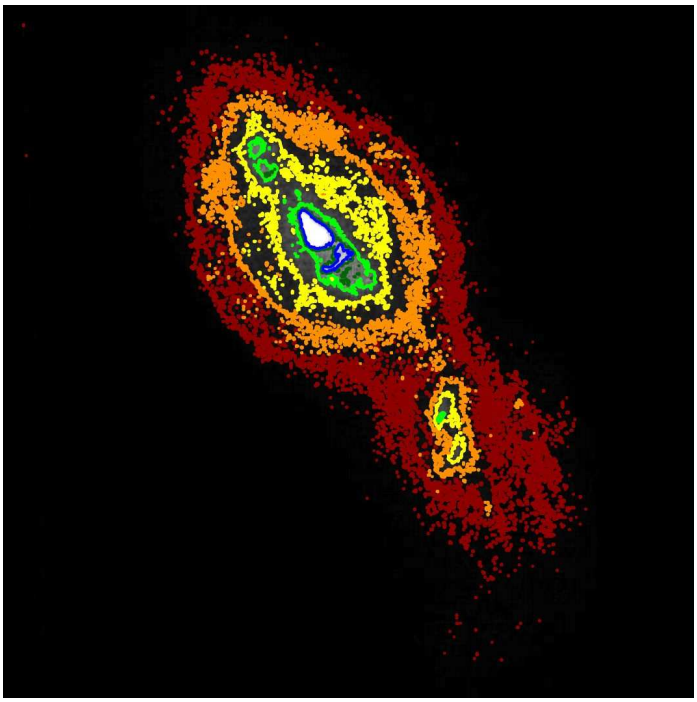

Figure 5.23: HST F253M 1993 image with the contours are on a logarithmic scale.

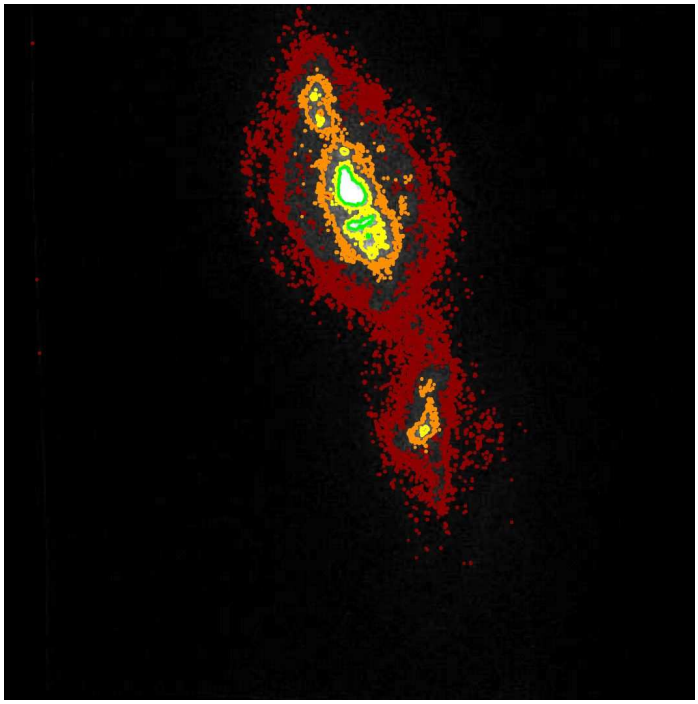

Figure 5.24: MHST F253M 1992 image with the contours are on a logarithmic scale.

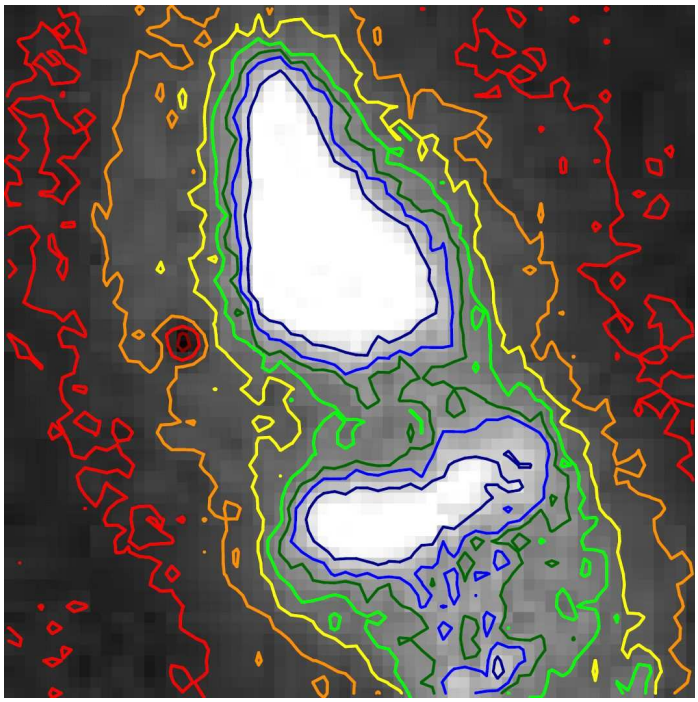

Figure 5.25: A zoomed in view of the inner arcsec of R Aqr. Here we see sources C1c and C1 really well. Source C2 appears to be more lopsided than the other sources. Looking to the right, one can notice that the right side seems to be slightly elongated like what we saw in the 2MASS images

Source	1992 F253M	1992 F190M	1992 F278M	1993 F253M
C1c	RA: $23^h43^m49.41^s$ Dec: $-15°17'4.4''$ 709.8 counts	RA: $23^h43^m49.42^s$ Dec: $-15°17'4.3''$ 379.5 counts	RA: $23^h43^m49.41^s$ Dec: $-15°17'4.4''$ 1708 counts	RA: $23^h43^m49.44^s$ Dec: $-15°17'3.6''$ 699.9 counts
C1	RA: $23^h43^m49.39^s$ Dec: $-15°17'4.6''$ 627 counts	RA: $23^h43^m49.4^s$ Dec: $-15°17'4.5''$ 204 counts	RA: $23^h43^m49.39^s$ Dec: $-15°17'4.6''$ 964 counts	RA: $23^h43^m49.43^s$ Dec: $-15°17'3.8''$ 638 counts
C1a+b	RA: $23^h43^m49.44^s$ Dec: $-15°17'3.9''$ 305 counts	RA: $23^h43^m49.44^s$ Dec: $-15°17'3.9''$ 94.7 counts	RA: $23^h43^m49.44^s$ Dec: $-15°17'3.9''$ 871 counts	RA: $23^h43^m49.47^s$ Dec: $-15°17'3.2''$ 191 counts
C2	RA: $23^h43^m49.46^s$ Dec: $-15°17'3.8''$ 259 counts	RA: $23^h43^m49.46^s$ Dec: $-15°17'3.8''$ 81 counts	RA: $23^h43^m49.46^s$ Dec: $-15°17'3.8''$ 752.7 counts	RA: $23^h43^m49.48^s$ Dec: $-15°17'3.1''$ 137 counts
A′	RA: $23^h43^m49.32^s$ Dec: $-15°17'5.5''$ 135 counts	RA: $23^h43^m49.33^s$ Dec: $-15°17'5.2''$ 60.49 counts	RA: $23^h43^m49.33^s$ Dec: $-15°17'5.5''$ 268 counts	RA: $23^h43^m49.36^s$ Dec: $-15°17'4.8''$ 107 counts
A1	RA: $23^h43^m49.61^s$ Dec: $-15°17'1.5''$ 128 counts	RA: $23^h43^m49.62^s$ Dec: $-15°17'1.4''$ 60.11 counts	RA: $23^h43^m49.61^s$ Dec: $-15°17'1.5''$ 265 counts	RA: $23^h43^m49.61^s$ Dec: $-15°17'0.6''$ 102 counts

Table 5.1: The counts and positions of the sources for each of the HST images.

5.4 3D Modeling of HST Images and Analysis

My next step was to create a 3D model of the images to show a better view of the peaks and distances between each peak. Using the IDL program, I launched the packet known as isurface to create a 3D surface image of each HST image. Upon first glance of the 3D surface model, I noticed that the central source would dominate the rest of the peaks. In order to get a better view of the lower peaks, I lowered the maximum counts that the package would detect. Figures 5.26 and 5.27 are examples of the 3D models created. With the central source lowered, the other source can be seen more easily. Within isurface, I was able to create a line profile over the direction of the sources which displays the source counts versus the pixel counts from the top of the picture. Figures 5.28 through 5.31 show the line profiles for each of the HST images.

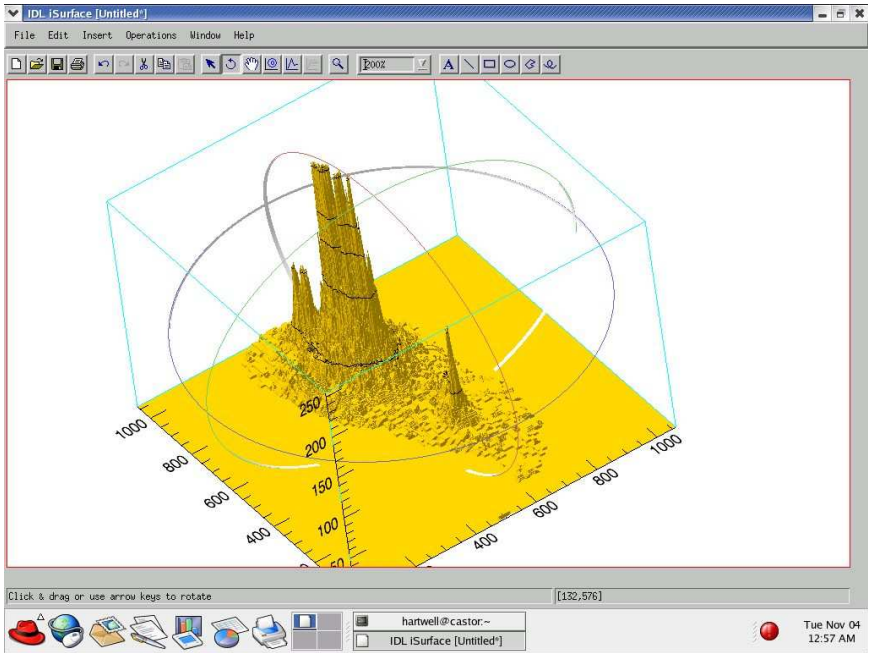

Figure 5.26: 3D model of HST F253M 1993 using isurface.

Using the line profiles, I was able to estimate the distances of each of the sources from each other. Assuming that the sources were on a perpendicular plane to the line of sight, I used the equation $a = 2\theta\,\pi\,d/360$ where a is the distance from stars to the source, d is the

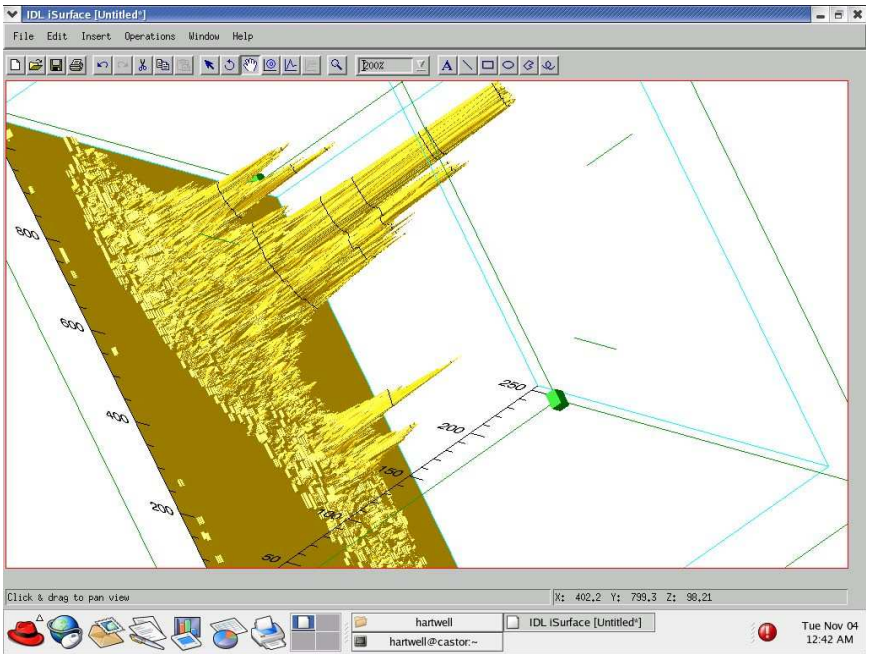

Figure 5.27: 3D model of HST F190M 1992 using isurface.

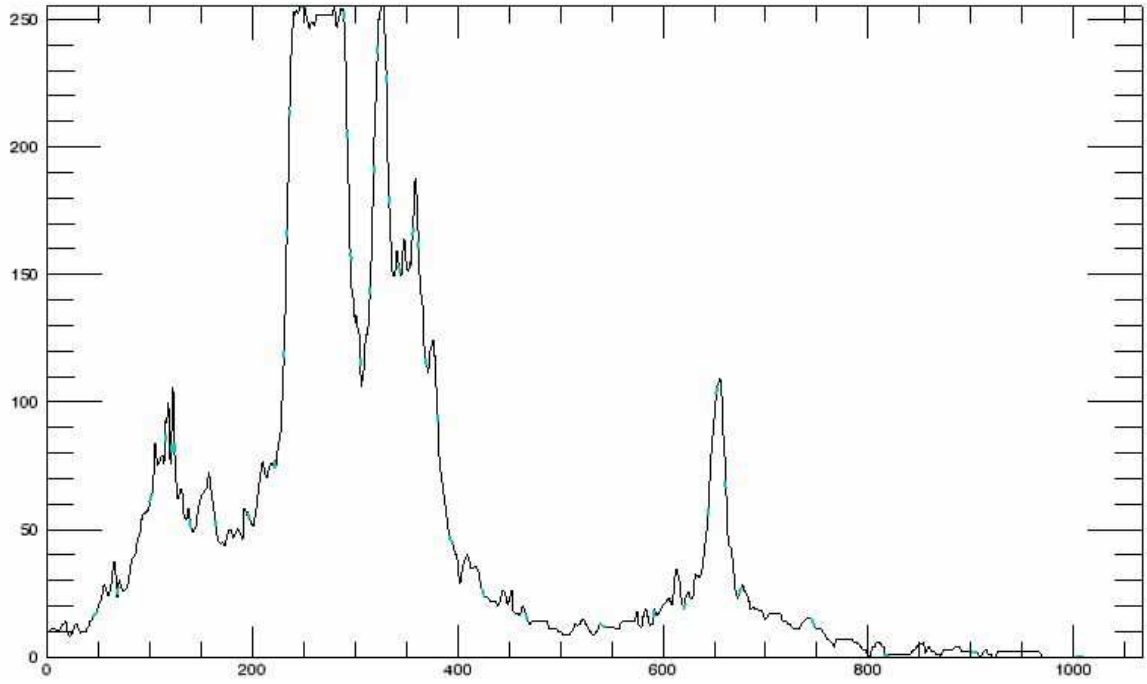

Figure 5.28: Line profile of HST F253M 1992.

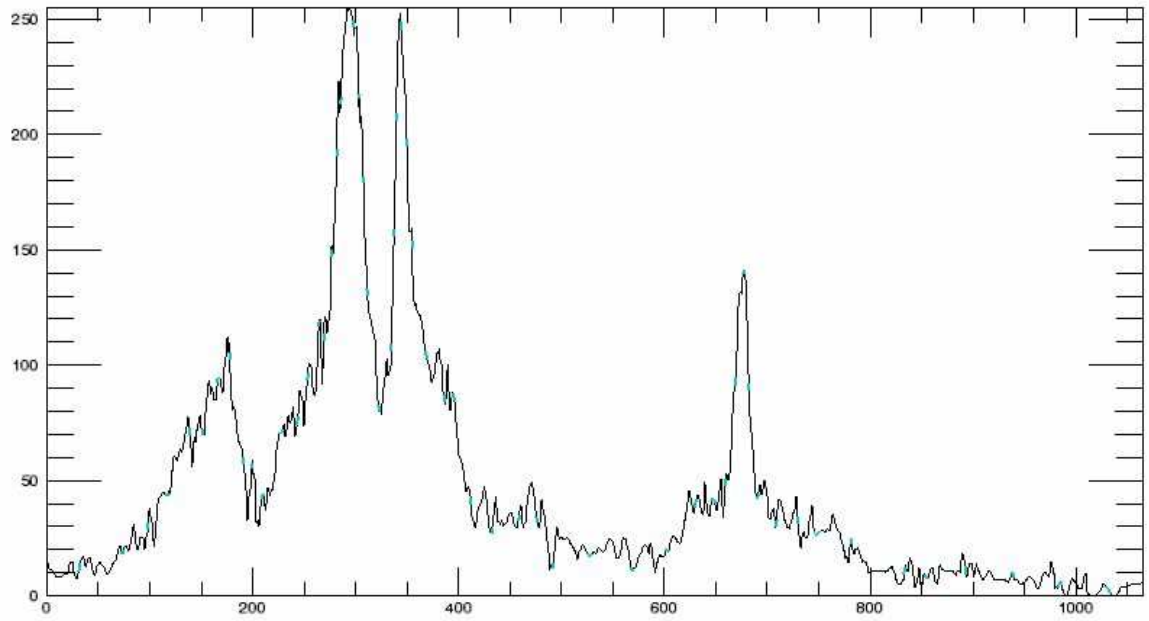

Figure 5.29: Line profile of HST F190M 1992.

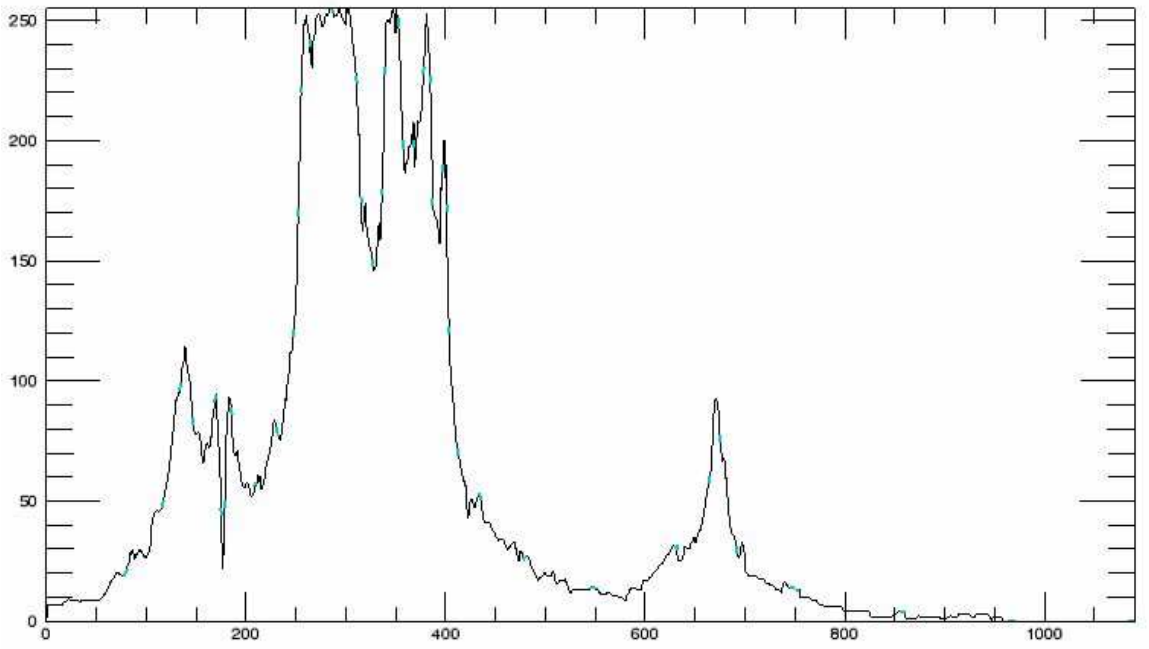

Figure 5.30: Line profile of F278M 1992.

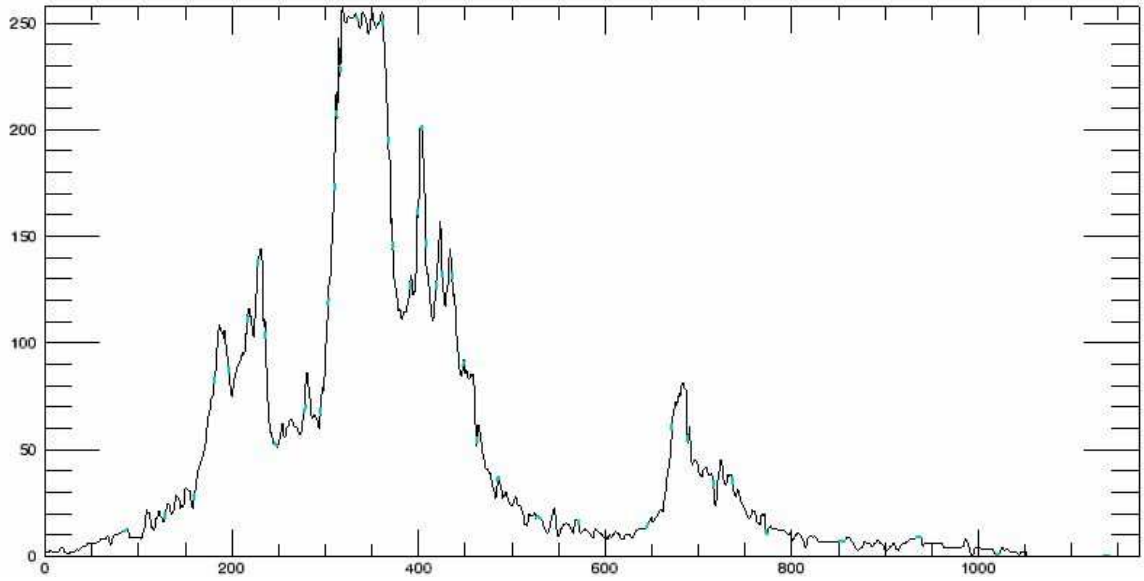

Figure 5.31: Line profile of HST F253M 1993.

distance to the plane which is assumed to be 220 ± 50 pc away (Hinkle et al., 1989), and θ is the angular distance between the stars and the source. I used the HST FOC conversion of 1 pixel = 0.0143 arcseconds to calculate θ. Table 5.2 shows the calculated distances from the line profiles in arcseconds, and Table 5.3 shows the calculated distances from the line profiles in AU. The errors in the distances in Table 5.3 come from error in the distance to the star and the error in the measurement of the sources. The error due to the source measurement was based on a Gaussian fit over the source and seeing what the offset is: ± 0.1 pixels (1.12 AU) for C1, ± 0.3 pixels (3.35 AU) for C1a+b, ± 0.5 pixels (5.59 AU) for C2, ± 7 pixels (78 AU) for A$'$, and ± 0.2 pixels (2.24 AU) for A1. Figure 5.32 shows a graph of the distances to each of the sources in each HST image.The first four sources are almost linear. A1 sadly breaks the linearity of the trend. A possibility for the greater distance of A1 is that a reverse shock is propagating in component A1. In this case, a collision with a cloud in front of A1 could cause the shock and subsequent disruption (Mäkinen et al., 2004).

With these distances and the information I have obtained, I can now compare my results to the models. In the next chapter I will finally scrutinize the different models proposed for R Aqr and which best matches my results as well as other authors.

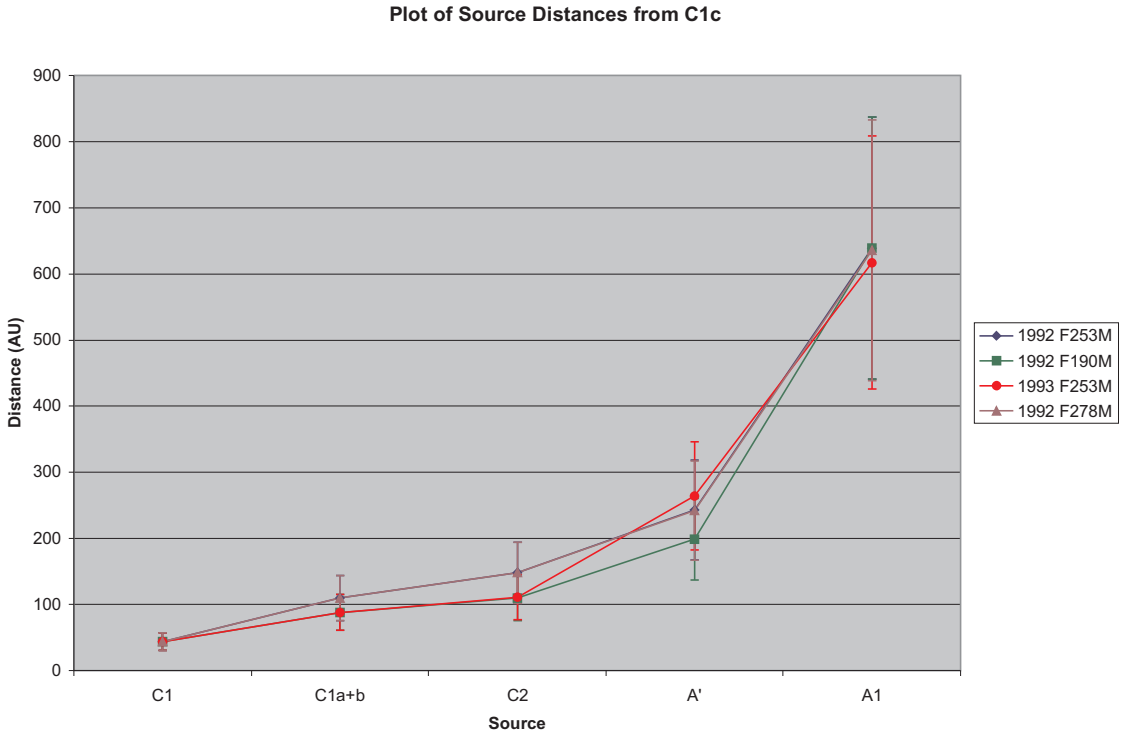

Figure 5.32: The distances each of the sources are away from the binary stars, C1c in AU.

Source	1992 F253M	1992 F190M	1992 F278M	1993 F253M
C1	0.201	0.201	0.201	0.201
C1a+b	0.501	0.401	0.501	0.401
C2	0.602	0.502	0.602	0.507
A′	1.104	0.905	1.103	1.203
A1	2.907	2.907	2.895	2.807

Table 5.2: The distances each of the sources are away from the binary stars, C1c in arcseconds

Source	1992 F253M	1992 F190M	1992 F278M	1993 F253M
C1	44 ± 5 AU	44 ± 7 AU	44 ± 4 AU	44 ± 7 AU
C1a+b	110 ± 10 AU	88 ± 14 AU	110 ± 7 AU	88 ± 16 AU
C2	148 ± 25 AU	110 ± 22 AU	148 ± 17 AU	111 ± 39 AU
A′	243 ± 33 AU	199 ± 39 AU	242 ± 46 AU	264 ± 68 AU
A1	639 ± 75 AU	639 ± 63 AU	636 ± 77 AU	617 ± 82 AU

Table 5.3: The distances each of the sources are away from the binary stars, C1c in AU.

CHAPTER 6. Modeling the R Aqr Jet

From Chapter 3, we found out what astronomers see in this star. However, these are just observations. So what do they mean? How do these observations relate to the nature of the star and most importantly the mysterious jet? In order to answer these questions, we must look to theoretical and computational models to give these observations meaning. Several models have been proposed for the R Aqr jet, but the three most prominent models are the Accretion Disk Model, the Parcel Model and the Collision of Winds Model. In this chapter I will compare each of the models to the observations seen in R Aqr and determine which model fits the best.

6.1 Nebular Models

Before going too deeply into the jet models, we must take into consideration the R Aqr system as a whole. The model proposed for the jets must not interfere with formation and structure of the nebulosity surrounding the two stars.

The complex nebula which surrounds the central star in a remarkably point-symmetric arrangement consists of two main components, the "inner" and "outer" nebulosity both discovered by Lampland (1922). The outer nebulosity is an oval-shaped formation of about $2'$ extent composed of two intersecting, well defined arcs and reminds the observer of a double convex lens oriented nearly east-west. Outward motions in the outer nebulosity were suspected by Hubble (Adams, 1942) and detected by Baade in 1944 (Osterbrock, 1996). They deduced an expansion age of about 600 yr and a kinematical distance of 260 pc.

With respect to the basic structure of the R Aqr nebula a number of questions have remained unanswered. The geometry of the expanding outer nebulosity is enigmatic. It cannot

be a planar, ring-like structure (seen nearly edge-on) as suggested by Wallerstein and Greenstein (1980), since the two arcs (considered to be the front and back halves of the "ring") extend beyond their intersections.

One physical mechanism for the formation of the outer nebula is that of a fast wind sweeping up inhomogeneously distributed ambient gas into a thin shell. Although the observed velocities of optical emission knots are well below that posited for the wind, this is to be expected since the low density and high temperature of the wind would result in it only being visible in UV resonance lines. Slight evidence for a fast wind in the system was found by Michalitsianos et al. (1988) from UV observations of CIV doublet ratios but in any case it may be that the wind is episodic and is not present at the current epoch. Winds of comparable speeds have been observed in other eruptive symbiotics during outbursts (Kwok et al., 1984). There is not yet an agreement on the driving mechanism for the hot wind. However, it has been suggested that radiation pressure in atomic lines, with mechanical heating at the base of the wind, could work (Drew and Verbunt, 1985). Another possibility for the fast wind is centrifugal driving along magnetic field lines (Pudritz et al., 1991).

It is likely that the ambient gas is material which was ejected during the red giant stage of the star that is now the white dwarf, and that this gas became predominantly concentrated in the orbital plane of the system. Although plausible models for the build up of this sort of density distribution exist in the case of close binaries that go through common envelope evolution (Livio and Soker, 1988), it is less clear how it can happen in a system with components as widely spaced as in R Aquarii. Nonetheless, it has been proposed that equatorial density enhancements can be caused by rotation of the wind progenitor or by the formation of an exterior "excretion disk" around the binary system (Morris, 1987).

A more exotic mechanism would be the "born again" disk formed from the destruction of a planetary system (Sahai et al., 1991). For comparison, many young stellar objects are found to show both small scale disks and large scale "interstellar toroids" whose axes are not necessarily aligned (Rodríguez, 1989). Also, from comparison of the number of planetary nebulae possessing close binary nuclei with the number showing bipolar morphology, it is apparent

that common envelope ejection cannot be the only mechanism able to produce a density contrast between equator and poles (Soker and Livio, 1989). The actual density distribution is not known, but the simplifying idea that the density is solely a function of distance from the orbital plane can be assumed.

6.2 Jet Models

In Chapter 2, Figure 2.3 shows two jets in the NE and SW from the central star. These jets first appeared between 1970 and 1977, in the form of a brilliant jet-like feature or spike extending approximately $10''$ toward position angle $\sim 24°$. So what causes these jets to occur? Several models have been proposed to explain these unusual jets. In this section are a few of the most well discussed models.

6.2.1 Parcel Model

The Parcel Model was first introduced by Hollis and Koupelis (2000). The model is based on the interaction of a hot isotropic stellar wind with a cooler cloud of gas. The hot wind creates a cavity of hot gas which escapes only through the direction of least resistance along the axis of rotation or the lines of magnetic field. Due to instabilities, the external boundaries of the bubble could evolve in nozzles leading to the formation of jets. Then, these jets may be further collimated by interaction with the external medium (Raga and Canto, 1989). They demonstrate how plasma parcels may be driven by a strong magnetic stellar rotator which could give rise to the observed nonrelativistic jet comprised of several discrete parcels in the R Aqr symbiotic system (see Figure 6.1). The model assumes the hot companion is embedded in a thick accretion disk, is rotating with an angular velocity Ω_0, and possesses a strong magnetic field that is confined to a narrow, cylindrically symmetric region (i.e. the "funnel") whose axis is coincident with the stellar rotational axis (which they have along the Z-axis). This region would be a disrupted hollow in the thick accretion disk. A parcel of "overaccreting" gas and dust could be expelled and accelerated along the funnel axis by radiation pressure, and would reach the injection point Z_0 with a velocity V_0. In any case, no matter how the parcel gets to

the injection point, Hollis and Koupelis's concern was modeling the Lorentz force components acting on the parcel. To account for the spacing between the sources in the jet, the model predicts that the hot companion precesses every ~ 18 yr. Their model accounts for observed velocities seen in both the radio and ultraviolet, and the helical structure seen in ultraviolet emission. This suggests a parcel structure with its ultraviolet emission forming a low-density sheath surrounding its radio region, which is denser by a factor of ~ 30.

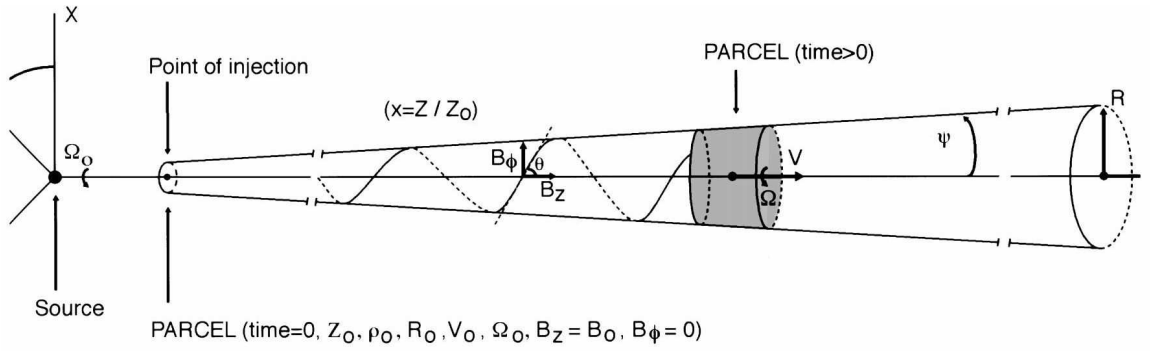

Figure 6.1: Schematic diagram of the jet parcel model (Hollis and Koupelis, 2000).

This model is good in theory, but there are some possible uncertainties that don't solidify this model as the true model for R Aqr. One such uncertainty is that none of their parameters were observationally confirmed. Their have been attempts to measure the magnetic flux of the jets (Wickramasinghe and Ferrario, 2000). Due to the assumed large separation, the companion in R Aqr can be classified as an isolated white dwarf. For isolated magnetic white dwarfs, the surface magnetic field strengths vary between 3×10^4–10^8 G. Hollis and Koupelis (2000) inferred the following surface magnetic field for the hot companion: $B_* = 9 \times 10^7$–4.6×10^9 G, if it is a subdwarf of radius 7×10^9 cm, and $B_* = 4.4 \times 10^9$–2.3×10^{11} G, if it is a white dwarf of radius of 10^9 cm. There inferred magnetic fields are higher than what should be expected according to Wickramasinghe and Ferrario (2000). A possible reason for this is because their model does not take into account any effect due to an accretion disk. However, they do not confirm the structure of the jets proposed in the parcel model or the numbers.

Also, according to Cotton et al. (2006), the magnetic fields appear to be oriented parallel to the features but due to the range of orientations seen in these features, their magnetic fields

are not part of a persistent, large scale dipole field.

Another uncertainty lies in the spacing of the sources. If the jet precesses every 18 years, we can roughly predict the spacing of the sources. In Table 5.1, the distances to the sources from C1c have been calculated using HST images. The distances for the precessing star do not match up as well as hoped shown in Table 5.2. Here Tables 6.1 and 6.2 compare my results with the parcel model and those made by other astronomers. The distances in Table 6.1 are measured using the distance modulus between the pixels (see Chapter 5 for discussion). The distances in Table 6.2 were measured using position measurements of the jet from Mäkinen et al. (2004) and Paresce and Hack (1994) as mentioned in their paper (Table 6.2). The distances are close, but the parcel model predicts lower distances than any of the observations made. Table 6.3 shows the χ-squared test of the measurements compared to that of the Parcel Model. This does make the difference in terms of where the sources are located since the χ-square show a number greater than 1 (which means it is less likely for these two observations to be similar).

Source	1992 F253M	1992 F190M	1992 F278M	1993 F253M	Parcel
C1	44 ± 5 AU	44 ± 7 AU	44 ± 4 AU	44 ± 7 AU	69 AU
C1a+b	110 ± 10 AU	88 ± 14 AU	110 ± 7 AU	88 ± 16 AU	161 AU
C2	148 ± 25 AU	110 ± 22 AU	148 ± 17 AU	111 ± 39 AU	159 AU
A$'$	243 ± 33 AU	199 ± 39 AU	242 ± 46 AU	264 ± 68 AU	200 AU
A1	639 ± 75 AU	639 ± 63 AU	636 ± 77 AU	617 ± 82 AU	721 AU

Table 6.1: Measured distances to each of the sources using HST images and those found by Hollis and Koupelis (2000).

Their model also does not take into account any effect due to an accretion disk or radiation hydrodynamics. The parcel must come from either the Mira or from the surrounding nebula. For a star that compact and is revolving around the Mira, material must be gathered near it in order to travel up the magnetic field lines. Also, to have the parcel emit in X-ray as seen in R Aqr, you must have either synchrotron or thermal bremsstrahlung radiation. For example, the thermal bremsstrahlung radiation seen in the radio regime is suggested as a relic of a passing shock front. Shock modeling of the R Aqr NE radio and UV jets suggests that temperatures

Source	Mäkinen	Paresce	Parcel
C1	40 AU	66 AU	69 AU
C1a+b	56 AU	166 AU	161 AU
C2	204 AU	202 AU	159 AU
A′	262 AU	278 AU	200 AU
A1	740 AU	762 AU	721 AU

Table 6.2: Distances measured by Mäkinen et al. (2004) (using $10' = 2000$ AU), Paresce and Hack (1994) (using $2.75'' = 550$ AU), and Hollis and Koupelis (2000).

1992 F253M	1992 F190M	1992 F278M	1993 F253M
3.22	2.31	3.09	2.13

Table 6.3: The reduced χ^2 numbers for each of the images compared to the Parcel model.

should be on the order of that required for X-ray emission.

6.2.2 Shock Model

Another way to explain the cause of the jets is through a shock model. The shock for the R Aqr system is created when a stream of gas is forced to change from supersonic motion (faster than the speed of sound) to subsonic motion (just under the speed of sound. This occurs when either when two supersonic winds collide or when a stream of gas collides with an accretion disk. The velocity and density change abruptly and the gas is compressed as it crosses the shock. The gas heats up and the temperatures can be high enough to display UV and X-ray radiation. One model that uses this concept is the collision of winds model which will be discussed next.

It was found that a shock wave travelling with 100 km s^{-1} could be a good model to explain the observational data, although some problems still remain (Hollis et al., 1991). In this case, the internal energy is approximately constant over the emission region. The resulting spectrum is characterized by X-ray emission and lines produced in high temperature conditions. In a radiative shock, the gas temperature varies relatively quickly over the emission region, and

the resulting spectrum depends on the detailed structure of the electron temperature and density in the shock front and relaxation region. The spectra of a radiative shock show a variety of mission lines of different ionization stages. A very large amount of data has been published on R Aqr, but due to the complexity and fast temporal evolution of this object simultaneous measurements are needed. Burgarella et al. (1992) and Hollis et al. (1991) tried to compare models to spectrophotometric data in order to get some indications on the emission line mechanisms in R Aqr.

6.2.3 Collision of Winds Model

Another process that could produce a jet is the collision of winds. Kwok et al. (1984) presented a model where an isotropic high velocity wind from the hot star interacts with the preexisting isotropic slower Mira wind. This leads to a high density nebular emission shell around the binary system. Soker and Livio (1989) introduced a model suggesting involving a density contrast between the equatorial and polar directions in the giant mass loss that would be due to the binary system. This scenario produces high density rings in the orbital plane, while the fast and hot wind will have higher velocities in the polar directions and produce a bow-shock when catches the slow, dense wind from the cool star. In the model of Willson et al. (1984) and Willson et al. (1984) proposed, the two winds collide head on creating turbulent flow and the gas escapes through a conical shell, where high ionization lines are produced. The continuous jet from the nucleus in the FOC images is certainly due to the same mechanism all along the filament up to $5''$ (2×10^{16} cm). The head on collision could thus produce the observed morphological arches seen in the nebulosity, and might be an important ingredient for the appropriate model of R Aqr. Using the mean values for the speed of the hot wind, $v_{\rm Mira} = 30$ km s^{-1} for the speed of the cool wind (Kenyon et al., 1988), and $-dM_{\rm Mira}/dt \sim 2.7 \times 10^{-7} M_{\odot}$ yr^{-1} also for the cool wind (Hollis et al., 1985), we can estimate the velocity ratio to be $w = v_{\rm hot}/v_{\rm Mira} = 28$ and the mass loss rate ratio $m = M_{\rm hot}/M_{\rm Mira} = 2.7 \times 10^{-4}$. Using these estimates, the parameter characterizing the geometric structure of the shell or interface, $mw \sim 7.5 \times 10^{-3}$, is bent towards the hot star,

eventually leading to an indented spheroidal nebula as seen in Figure 6.2 (Girard and Willson, 1987).

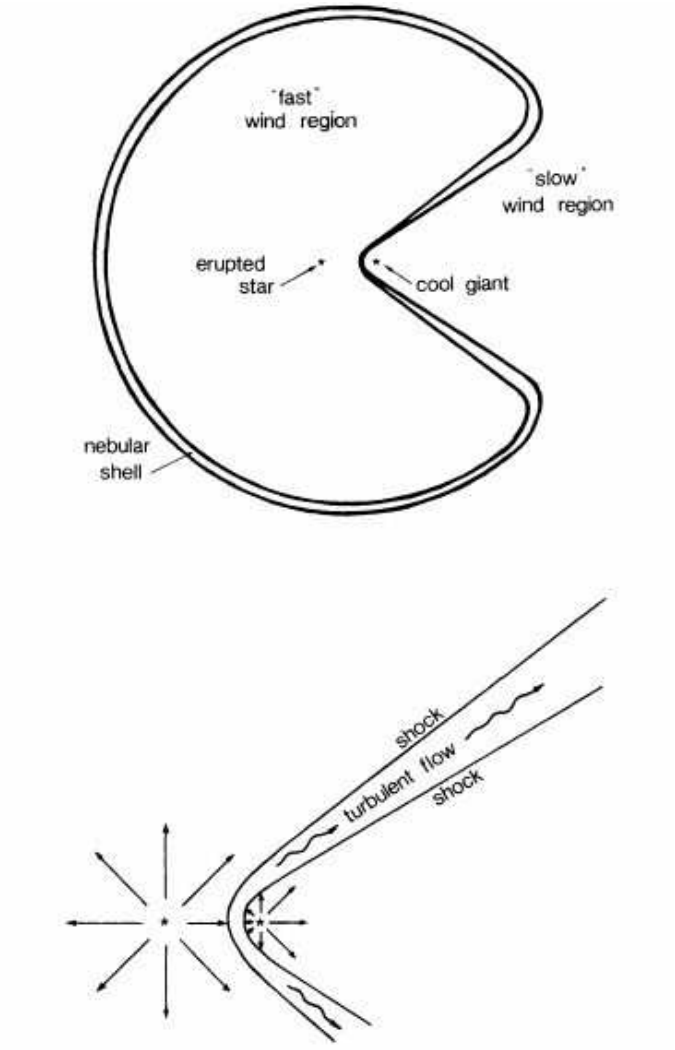

Figure 6.2: Proposed colliding wind model for eruptive symbiotics (Girard and Willson, 1987).

Since the two stars revolve around each other, the turbulent flow will get swept up into a spiral structure. Observing this spiral edge on, we would be able to see bright sources created when the turbulent flow would be the thickest. Figure 6.3 best displays this concept. You see the gradual decay of the sources as you become more distant from the central source. The line profiles in Chapter 5 show us this gradual decay. The distances to each source can be measured assuming the winds expand at a constant rate. The distances to each source can be

measured assuming the winds expand at a constant rate. The distances to each of the sources can are calculated in Table 6.4 given the speed of the propagating wind to be ~ 3 AU year^{-1} (Mäkinen et al., 2004) and the time scale of propagation to be ~ 15 years (Mäkinen et al., 2004). Most of the sources fit well with the distances, except for source A1. A possibility for the greater distance is that a reverse shock is propagating in component A1. In this case, a collision with a cloud in front of A1 could cause the shock and subsequent disruption (Mäkinen et al., 2004). With this in mind, I removed source A1 from the possibilities of χ-square fits as seen in Table 6.5. With the first four sources, the χ-square numbers are close to one, which indicate that the observational distances fit the model distances.

Source	1992 F253M	1992 F190M	1992 F278M	1993 F253M	Parcel
C1	44 ± 5 AU	44 ± 7 AU	44 ± 4 AU	44 ± 7 AU	45 AU
C1a+b	110 ± 10 AU	88 ± 14 AU	110 ± 7 AU	88 ± 16 AU	111 AU
C2	148 ± 25 AU	110 ± 22 AU	148 ± 17 AU	111 ± 39 AU	177 AU
A$'$	243 ± 33 AU	199 ± 39 AU	242 ± 46 AU	264 ± 68 AU	243 AU
A1	639 ± 75 AU	639 ± 63 AU	636 ± 77 AU	617 ± 82 AU	309 AU

Table 6.4: Measured distances to each of the sources using HST images and the calculated distances using the Collision of Winds model.

1992 F253M	1992 F190M	1992 F278M	1993 F253M
0.47	0.62	0.85	0.93

Table 6.5: The reduced χ^2 numbers for each of the images compared to the Collision of Winds model.

However, there are some uncertainties to this model. The model assumes that the wind expands at a constant rate. With the nebula surrounding the star, the wind would collide with the nebulosity and the distances would be inconsistent. Also, if the wind interacts with the Interstellar Medium (ISM) again the distance would be inconsistent. This is hard to conceive since there are many variables to take into consideration (temperature of the wind, wind speed, density of the nebulosity, temperature of the nebulosity, speed of the expanding nebulosity,

etc.). But, hydrodynamical simulations of R Aqr using colliding winds could be created to take all of these into account. Sadly, no such simulations have yet been created for R Aqr specifically. However, there are papers that model other systems that demonstrate colliding winds (see, e.g., Parkin and Pittard, 2008; Kenny and Taylor, 2007; Bogovalov et al., 2008). These models could be used with R Aqr.

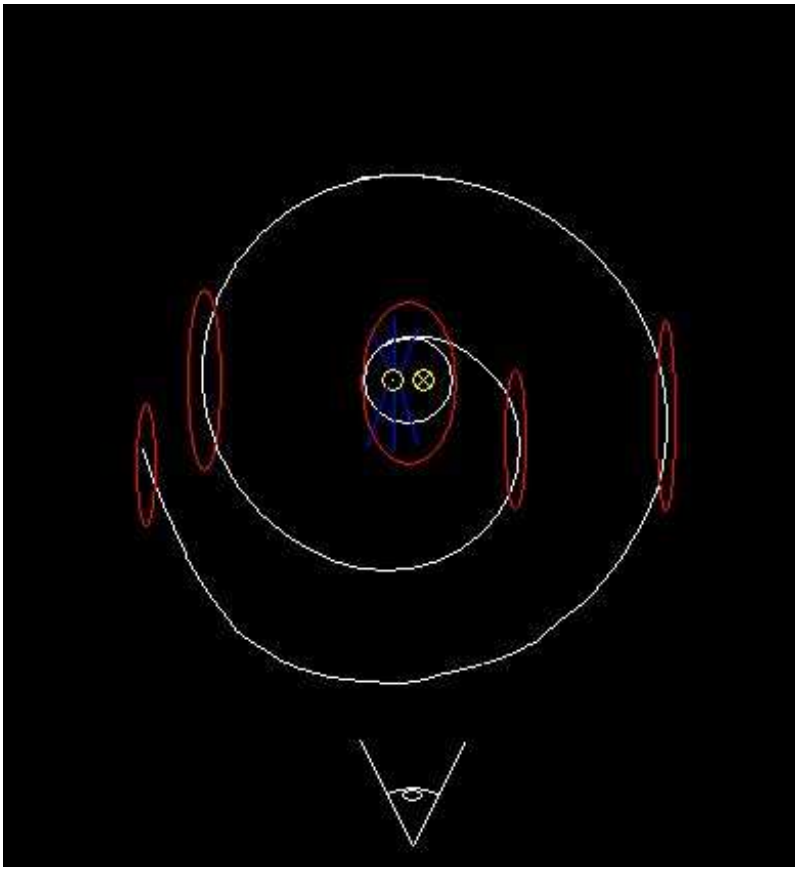

Figure 6.3: The turbulent flow would be swept into a spiral structure similar to what is displayed here. The red ovals indicate where the observer would view the most turbulent flow down the "edge" of each spiral. With each progressive "edge" away from the stars, the sources would get fainter.

6.2.4 Accretion Disk Model

The Accretion Disk Model holds that an accretion disk is created around the hot companion and the jets are formed by the heating of the disk. In this model, an accretion disk is responsible

for the central photons needed to explain the observed nebular emission. However, there are two ways to create this concept. One way is to have both of the stars are on highly eccentric orbits around each other. When the two stars reach periastron (the closest point the can get in their orbits), an accretion disk can be formed. If the stars are close enough to each other, a phenomenon known as Roche Lobe Overflow (RLOF) occurs. RLOF happens when the hot companion enters the Roche limit (the point where the star begin to feel the strain of tidal forces from the companion) of the Mira. The Mira then becomes an elongated sphere and begins to transfer mass onto the hot companion. The material transferred forms a disk around the companion and starts accreting material on to the companion. The companion will heat of the material and if enough material accumulates, it will create a sudden eruption. These bursts have been seen in R Aqr by the Koreans in 1074 AD (Yang et al., 2005). They predict a 500 year eruption period for the star. Figure 6.4 displays the orbits of the stars and Figure 6.5 shows an artist's rendition of R Aqr with RLOF. Another way to create the disk is to have

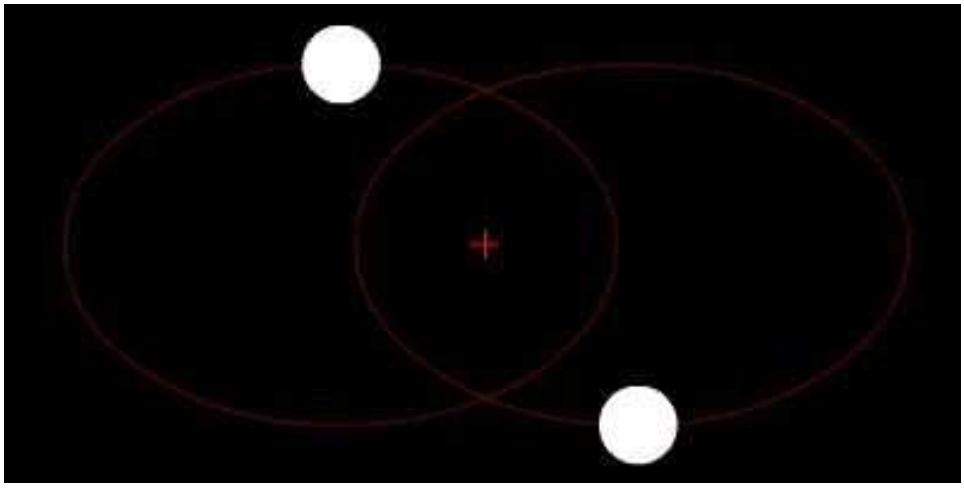

Figure 6.4: Two stars in elliptical orbits around a common center of gravity. The two stars will be close enough to have RLOF when they approach the closest to each other (periastron). This model is not to scale for R Aqr, but is a good representation of this type of orbit.

the stars in circular orbits around each other where the orbits don't get close enough to create RLOF. Figure 6.6 best demonstrates this kind of orbit. The accretion disk is created when the winds from the pulsating Mira gets caught up by the orbiting companion (which doesn't show

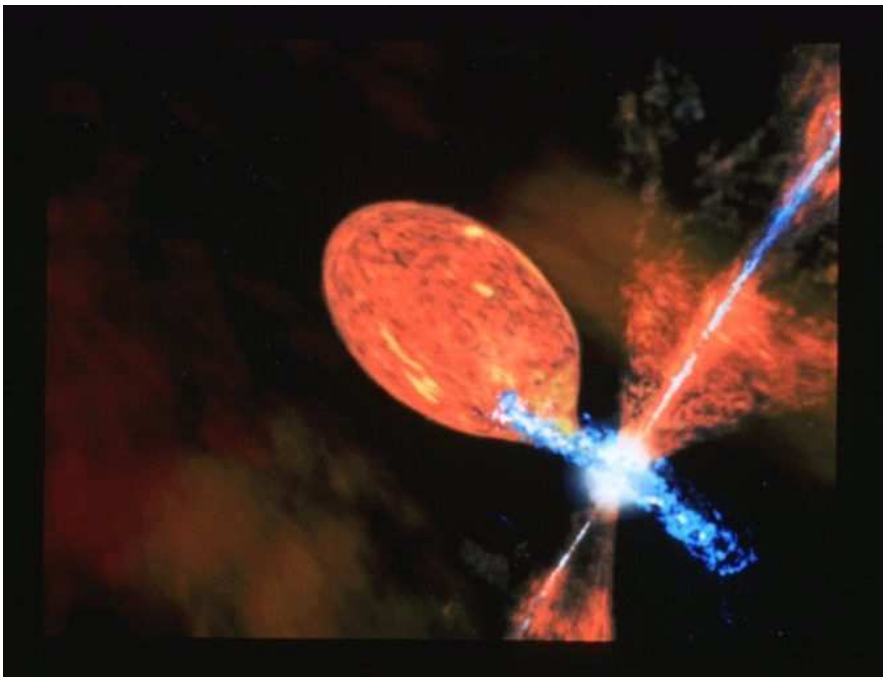

Figure 6.5: Dana Berry's rendition of R Aqr.

to have a wind). Since the companion is revolving around the center, the material sent out by the Mira gets pulled in by angular acceleration.

Hollis et al. (1985) derived the mass loss rate from the Mira to be $\sim 2.7\times10^{-7}M_{\odot}$ yr^{-1} from their radio images and the model mentioned in their paper. Burgarella et al. (1992) found that the accretion disk or the boundary layer must be a photon source with a radiation temperature $\sim 5 \times 10^4$ K and luminosity $\sim 10L_{\odot}$. If the accretion rate is $10^{-8}M_{\odot}$ yr^{-1} (Kafatos et al., 1986), the efficiency of converting accretion energy to photons is about 5%, a rather high value considering the separation between the components, which is presumably larger than 13 AU. However, if no accretion disk is formed, the accreted gas flows essentially in free-fall on to the stellar surface. In order to be accreted, the inflowing gas must be decelerated, resulting in a strong shock which produce a hard X-ray emission mainly due to bremsstrahlung. However, R Aquarii is only known as a weak soft X-ray emitter as expected if an accretion disk appears (Viotti et al., 1987).

Like the prior models, there are complications that need to be addressed. The first un-

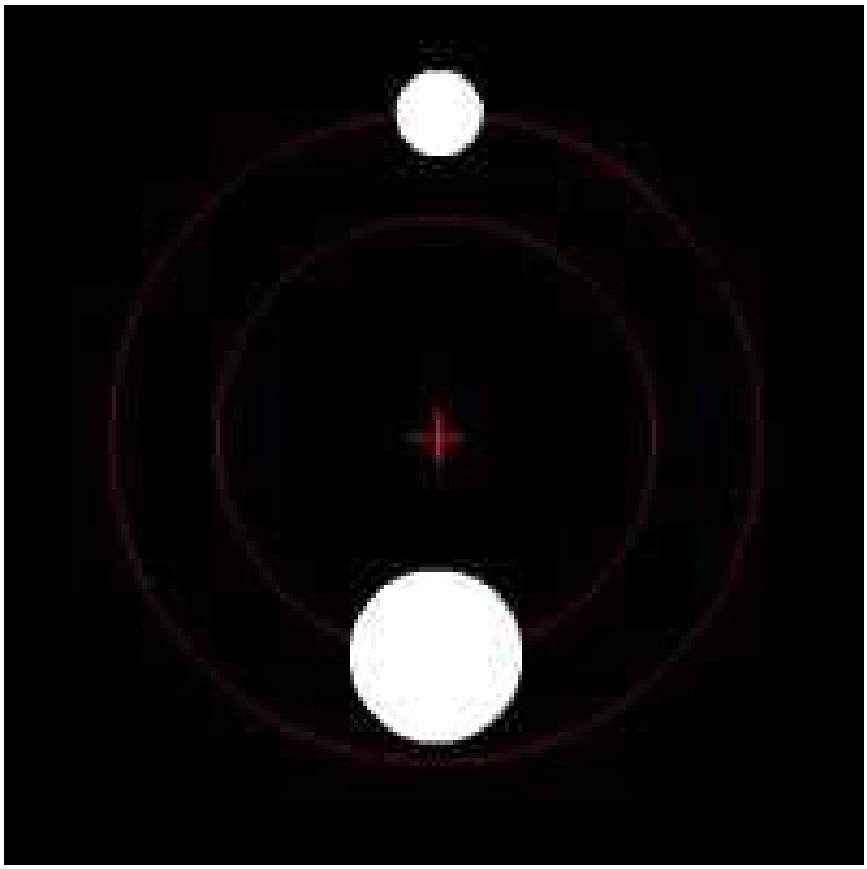

Figure 6.6: Two stars in circular orbits around a common center of gravity. The two stars will never be close enough to have RLOF if they orbit around the center at the same rate. This model is not to scale for R Aqr, but is a good representation of this type of orbit.

certainty lies in the measurement of the temperature. Livio and Soker (1988) predicted the temperature of the accretion for this type of binary to be around 30,000 K. This condition shows that a quasi-steady accretion disk can form from capture of a stellar wind in R Aqr. In this scenario, we expect an accretion disk to be responsible for the jet outflow and also for the central photon source needed to explain the observed nebular emission However, Kaler (1981) measured the radiation temperature of the disk to be 50,000 K. A disk temperature of about 30,000 K would be accompanied by a much higher boundary layer temperature, and the luminosity released in this boundary layer would be similar to the disk luminosity. Thus, an accretion disk seems to be inconsistent with the data. The difference of the temperature is almost a factor of 2 which means that there must be something else going on with the system.

A second problem has to deal with the positions of the sources and their intensities. For a 500 year eruption rate, the sources would have greatly decayed by the time the next one would occur. The source counts measured in Table 5.2 show a steady decline from the central stars. These counts seem inconsistent with the 500 year time period between eruptions.

Another concern lies with the orientation of the jet itself. The jet is tilted 29° from the plane of the nebular structure surround it. For a typical accretion disk, the jets would lie perpendicular to the plane. For such a large angle of tilt, there must be something else going on.

6.3 Conclusions

R Aqr has been studied for almost 100 years and even today it is continually being studied in hopes to reveal the mysteries behind this binary. It has been observed in many different mediums and slowly its features are being discovered. In this paper, I only used images taken by HST taken in 1992 and 1993. However, newer images from different telescopes are available. As mentioned in Chapter 3, different wavelengths and observations reveal different bits of information. It would be good to continue to further this study with different images and taken at different times.

Nonetheless, after analyzing the possibilities and putting each model under much scrutiny, it is hard to say which model is the "true" representation of R Aqr. Each model has strengths and some uncertainties. Also, time is a factor against us. We have to take observations over the course of 18, 44, or 500 years (given the model). However, the model that shows the most potential is the collision of winds model. The hindrances for this model can be overcome and there are no observations that prove it wrong. By creating the hydrodynamical simulations, with ISM and wind calculations taken into account, the model could be more of a likely candidate. In conclusion, the best model to describe R Aqr currently is the collision of winds model.

Acknowledgements

Behind every great student are great people who support and aid them. This paper would not be possible without the help of several individuals. Dr. Lee Anne Willson took me on as a lost student and patiently guided me down the path of proper research and scientific writing. Dr. Charles Kerton aided with the production of the results by guiding me through IDL protocol and terminology. Chris Anderson aided by retrieving information, guided me to several resources I could use, and helped me contact Eddie Bergeron, currently working with HST. David Malin provided the beautiful image of R Aquarii taken with the Anglo-Australian Observatory also seen in this paper. Martin Schroedter helped with translation of two of the papers used in the database. Jason Ekstrand helped me create a movie of the precessing motions of R Aqr used in my presentation. My parents have been with me throughout my college career, and have supported me greatly. My loving husband, Daniel, was my strongest supporter and helped me keep going when I would be so deep into my research. Ryan Wesley Tobin, Arun Madhavan, and Tom Stroman supported my efforts, kept me honest, and provided well needed intellectual breaks.

Bibliography

Adams, W. S.: 1942, *Mount Wilson Observatory Annual Report* **14**, 3

Anandarao, B. G. and Pottasch, S. R.: 1986, A&A **162**, 167

Aspin, C. and Schwarz, H. E.: 1988, *Polarimetry of the R Aquarii system*, pp 403–432

Bogovalov, S. V., Khangulyan, D. V., Koldoba, A. V., Ustyugova, G. V., and Aharonian, F. A.: 2008, MNRAS **387**, 63

Burgarella, D., Vogel, M., and Paresce, F.: 1992, A&A **262**, 83

Cotton, W. D., Vlemmings, W., Mennesson, B., Perrin, G., Coudé Du Foresto, V., Chagnon, G., Diamond, P. J., van Langevelde, H. J., Bakker, E., Ridgway, S., Mc Allister, H., Traub, W., and Ragland, S.: 2006, A&A **456**, 339

Deshpande, M. R., Joshi, U. C., Kulshrestha, A. K., Sen, A. K., Rao, N. K., and Raveendran, A. V.: 1987, PASP **99**, 62

Drew, J. and Verbunt, F.: 1985, MNRAS **213**, 191

Garnavich, P. M.: 1981, *Journal of the American Association of Variable Star Observers (JAAVSO)* **10**, 60

Giacconi, R., Gursky, H., Paolini, F. R., and Rossi, B. B.: 1962, *Physical Review Letters* **9**, 439

Girard, T. and Willson, L. A.: 1987, A&A **183**, 247

Graff, K.: 1920, *Astronomische Nachrichten* **210**, 61

Gray, M. D., Ivison, R. J., Humphreys, E. M. L., and Yates, J. A.: 1998, MNRAS **295**, 970

Gregory, P. C. and Seaquist, E. R.: 1974, Nature **247**, 532

Hinkle, K. H., Wilson, T. D., Scharlach, W. W. G., and Fekel, F. C.: 1989, AJ **98**, 1820

Hollis, J. M. and Koupelis, T.: 2000, ApJ **528**, 418

Hollis, J. M., Michalitsianos, A. G., Kafatos, M., and McAlister, H. A.: 1985, ApJ **289**, 765

Hollis, J. M., Michalitsianos, A. G., Kafatos, M., Wright, M. C. H., and Welch, W. J.: 1986, ApJ **309**, L53

Hollis, J. M., Oliversen, R. J., Michalitsianos, A. G., Kafatos, M., and Wagner, R. M.: 1991, ApJ **377**, 227

Hollis, J. M., Oliversen, R. J., and Wagner, R. M.: 1989, ApJ **337**, 795

Isles, J. E.: 1994, S&T **88(4)**, 74

Kafatos, M., Hollis, J. M., Yusef-Zadeh, F., Michalitsianos, A. G., and Elitzur, M.: 1989, ApJ **346**, 991

Kafatos, M., Michalitsianos, A. G., and Hollis, J. M.: 1986, ApJS **62**, 853

Kaler, J. B.: 1981, ApJ **245**, 568

Kenny, H. T. and Taylor, A. R.: 2007, ApJ **662**, 1231

Kenyon, S. J., Fernandez-Castro, T., and Stencel, R. E.: 1988, AJ **95**, 1817

Kwok, S., Bignell, R. C., and Purton, C. R.: 1984, ApJ **279**, 188

Lampland, C. O.: 1922, PASP **34**, 218

Livio, M. and Soker, N.: 1988, ApJ **329**, 764

Mäkinen, K., Lehto, H. J., Vainio, R., and Johnson, D. R. H.: 2004, A&A **424**, 157

Mattei, J. A. and Allen, J.: 1979, JRASC **73**, 173

Merrill, P. W.: 1919, PASP **31**, 305

Merrill, P. W.: 1950, ApJ **112**, 514

Michalitsianos, A. G. and Kafatos, M.: 1982, ApJ **262**, L47

Michalitsianos, A. G., Kafatos, M., Fahey, R. P., Viotti, R., Cassatella, A., and Altamore, A.: 1988, ApJ **331**, 477

Morris, M.: 1987, PASP **99**, 1115

Nikitin, S. N. and Khudyakova, T. N.: 1979, *Soviet Astronomy Letters* **5**, 327

Osterbrock, D. E.: 1996, *Journal for the History of Astronomy* **27**, 301

Paresce, F., Albrecht, R., Barbieri, C., Blades, J. C., Boksenberg, A., Crane, P., Deharveng, J. M., Disney, M. J., Jakobsen, P., Kamperman, T. M., King, I. R., Macchetto, F., Mackay, C. D., Weigelt, G., Baxter, D., Greenfield, P., Jedrzejewski, R., Nota, A., and Sparks, W. B.: 1991, ApJ **369**, L67

Paresce, F. and Hack, W.: 1994, A&A **287**, 154

Parkin, E. R. and Pittard, J. M.: 2008, MNRAS **388**, 1047

Pudritz, R. E., Pelletier, G., and Gomez de Castro, A. I.: 1991, in C. J. Lada and N. D. Kylafis (eds.), *NATO ASIC Proc. 342: The Physics of Star Formation and Early Stellar Evolution*, pp 539–+

Raga, A. C. and Canto, J.: 1989, ApJ **344**, 404

Rodríguez, L. F.: 1989, in G. Tenorio-Tagle, M. Moles, and J. Melnick (eds.), *IAU Colloq. 120: Structure and Dynamics of the Interstellar Medium*, Vol. 350 of *Lecture Notes in Physics, Berlin Springer Verlag*, pp 197–+

Sahai, R., Wootten, A., Schwarz, H. E., and Clegg, R. E. S.: 1991, A&A **251**, 560

Shakovskoi, N. M.: 1969, *Izv. Krymskoy Astrofiz. Obs.* **132**, 370

Shore, S. N., Michalitsianos, A. C., and Kafatos, M.: 1992, in L. Drissen, C. Leitherer, and A. Nota (eds.), *Nonisotropic and Variable Outflows from Stars*, Vol. 22 of *Astronomical Society of the Pacific Conference Series*, pp 308–+

Soker, N. and Livio, M.: 1989, ApJ **339**, 268

Solf, J. and Ulrich, H.: 1983, *Mitteilungen der Astronomischen Gesellschaft Hamburg* **60**, 318

Solf, J. and Ulrich, H.: 1985, A&A **148**, 274

Sopka, R. J., Herbig, G., Michalitsianos, A. G., and Kafatos, M.: 1982, ApJ **258**, L35

Viotti, R., Piro, L., Friedjung, M., and Cassatella, A.: 1987, ApJ **319**, L7

Wallerstein, G. and Greenstein, J. L.: 1980, PASP **92**, 275

Whitelock, P. A.: 1987, PASP **99**, 573

Wickramasinghe, D. T. and Ferrario, L.: 2000, PASP **112**, 873

Willson, L. A., Garnavich, P., and Mattei, J. A.: 1981, *Information Bulletin on Variable Stars* **1961**, 1

Willson, L. A., Wallerstein, G., Brugel, E. W., and Stencel, R. E.: 1984, A&A **133**, 154

Yang, H.-J., Park, M.-G., Cho, S.-H., and Park, C.: 2005, A&A **435**, 207

Zirin, H.: 1976, Nature **259**, 466